Atmos. Meas. Tech. Discuss., doi:10.5194/amt-2016-345, 2016
Manuscript under review for journal Atmos. Meas. Tech.
Published: 14 November 2016

Atmospheric Measurement Techniques Discussions

Long term assessment of the CALIPSO Imaging Infrared Radiometer (IIR) calibration and stability through comparisons with MODIS/Aqua and SEVIRI/Meteosat

Anne Garnier[1,2], Noëlle A. Scott[3], Jacques Pelon[4], Raymond Armante[3], Laurent Crépeau[3], Bruno Six[5], Nicolas Pascal[6]

1 Science Systems and Applications, Inc., Hampton, VA 23666, USA

[2] NASA Langley Research Center, Hampton, VA 23681, USA

[3] Laboratoire de Météorologie Dynamique, Ecole Polytechnique-CNRS, Palaiseau, 91128, France

[4] Laboratoire Atmosphères, Milieux, Observations Spatiales, UPMC-UVSQ-CNRS, Paris, 75252, France

[5] Université Lille 1, AERIS/ICARE Data and Services Center, Lille, 59650, France

[6] Hygeos, AERIS/ICARE Data and Services Center, Lille, 59650, France

Correspondence to: Anne Garnier (anne.garnier@latmos.ipsl.fr)

Abstract

The quality of the calibrated radiances of the medium-resolution Imaging Infrared Radiometer (IIR) on-board the CALIPSO satellite is quantitatively controlled since the beginning of the mission in June 2006. Two complementary "relative" and "stand-alone" approaches are used, which are related to comparisons of measured brightness temperatures, and to model-to-observations comparisons, respectively. In both cases, IIR channels 1 (8.65 μm), 2 (10.6 μm), and 3 (12.05 μm) are paired with MODIS/Aqua "companion" channels 29, 31, and 32, respectively, as well as with SEVIRI/Meteosat companion channels IR8.7, IR10.8 and IR12, respectively. These pairs were selected before launch to meet radiometric, geometric and space-time constraints. The pre-launch studies were based on simulations and sensitivity studies using the 4A/OP radiative transfer model fed with the more than 2300 atmospheres of the climatological TIGR dataset further sorted out in five air mass types. Over the 9.5 years of operation since launch, in a semi-operational process, collocated measurements of IIR and of its companion channels have been compared at all latitudes over ocean, during day and night, and for all types of scenes in a wide range of brightness temperatures when dealing with the relative approach. The relative approach shows an excellent stability of IIR2-MODIS31 and IIR3-MODIS32 brightness temperature differences (BTD) since launch A slight trend of the IIR1-MODIS29 BTD, equal to -0.02 K/year on average over 9.5 years, is detected by the relative approach at all latitudes and all scene temperatures. For the stand-alone approach, clear sky measurements only are considered, which are directly compared with simulations using 4A/OP and collocated ERA-Interim reanalyses. The clear sky mask is derived from collocated observations from IIR and the CALIPSO lidar. Simulations for clear sky pixels in the tropics reproduce the differences between IIR1 and MODIS29 within 0.02 K, and between IIR2 and MODIS31 within 0.04 K, whereas IIR3-

Atmos. Meas. Tech. Discuss., doi:10.5194/amt-2016-345, 2016
Manuscript under review for journal Atmos. Meas. Tech.
Published: 14 November 2016

Atmospheric Measurement Techniques Discussions

MODIS32 is larger than simulated by 0.26 K. The stand-alone approach indicates that the trend identified from the relative approach originates from MODIS29, whereas no trend (less than ± 0.004 K/year) is evidenced for any of the IIR channels. Finally, a year-by-year seasonal bias between nighttime and daytime IIR-MODIS BTDs was found at mid-latitude in the northern hemisphere by the relative approach. It is due to a nighttime IIR bias as determined by the stand-alone approach, which originates from a calibration drift during day-to-night transitions. The largest bias is in June/July with IIR2 and IIR3 too warm by 0.4 K on average, and IIR1 too warm by 0.2 K.

1 Introduction

The Cloud-Aerosol Lidar and Infrared Pathfinder Satellite Observation (CALIPSO) satellite (Winker et al., 2010), launched in April 2006, carries CALIOP (Cloud-Aerosol Lidar with Orthogonal Polarization), a visible camera, and the Imaging Infrared Radiometer (IIR). IIR was built in France by the Centre national d'Etudes Spatiales (CNES), the Société d'Etudes et de Réalisations Nucléaires (SODERN), and Institut Pierre Simon Laplace (IPSL) (Corlay et al., 2000). It includes three spectral bands in the thermal infrared atmospheric window, at 8.65 µm (IIR1), 10.6 µm (IIR2) and 12.05 µm (IIR3) with bandwidths of 0.85 µm, 0.6 µm, and 1 µm, respectively. These three channels were chosen to optimize retrievals of ice clouds properties in synergy with collocated observations from the CALIOP lidar (Garnier et al., 2012, 2013).

It is now well recognized by the international community that to be fully useful for climate and environmental applications, satellite observations require quality control during the instruments lifetime. Indeed, any systematic error or spurious trend not identified in the calibrated radiances may induce artefacts in the retrieved variables. As soon as in the mid- 1990's, the NOAA/NASA Pathfinder Program and later on in 2005 the Global Space-Based Inter-Calibration System (GSICS) initiated international collaborative efforts to improve and harmonize the quality of observations from operational weather and environmental satellites in order to create climate data records (e.g. Goldberg et al., 2011). A recent update on the GSICS vision is given in a 2015 WMO (World Meteorological Organization) report (GSICS, 2015).

In this paper, IIR observations are controlled and characterized since launch using two complementary approaches, which are the heritage of the processing of numerous years of satellite radiances for the restitution of climate variables (Chédin et al, 1985 and papers onwards on similar topics referenced and regularly updated at http://ara.abct.lmd.polytechnique.fr/index.php?page=publications). The monitoring of observational and computational biases or trends over long periods of time started with the NOAA/NASA TOVS (Tiros Operational Vertical Sounder) Pathfinder Program (Chédin et al., 1985; Scott et al., 1999). Since then, it has been implemented for more recent hyperspectral sounders, namely the Atmospheric Infrared Sounder (AIRS) on board Aqua since 2003, and since 2007 the Interféromètre Atmosphérique de Sondage Infrarouge (IASI) implemented on MetOpA and MetOpB (this latter in cooperation with CNES (e.g. Jouglet et al., 2014) within the frame of its GSICS activities).

The first approach, called "relative approach", is based on a channel to channel inter-comparison of radiances, further converted into equivalent brightness temperatures, with collocated measurements in companion channels of companion

Atmos. Meas. Tech. Discuss., doi:10.5194/amt-2016-345, 2016
Manuscript under review for journal Atmos. Meas. Tech.
Published: 14 November 2016

instruments under controlled conditions. The relative approach, sometimes referred to as "inter-channel" or "inter-calibration" approach, was initially developed in a GEO-LEO (GEOstationary-Low Earth Orbit) combination for the calibration of Meteosat-1, based on space and time collocations with TOVS on the NOAA Tiros-N series (Bériot et al., 1982). The second approach, called "stand-alone" approach is based on comparisons between measured and simulated brightness temperatures for each companion channel of each companion instrument. The two approaches are complementary: the inter-calibration approach - addressing any type of clear or cloudy scenes - allows a wide range of brightness temperatures to be studied while analysing the behaviour of one channel relative to its companion. The stand-alone approach screens each channel of each instrument, individually, for clear sky scenes. It contributes identifying which channel deviates from the other(s).

The IIR companion instruments chosen for this study are MODIS (Moderate Resolution Imaging Spectroradiometer) on board Aqua, and SEVIRI (Spinning Enhanced Visible and Infrared Imager) on board the geostationary second generation satellites Meteosat 8, 9, and 10. Both the MODIS and SEVIRI instruments, in operation since 2002 and 2004, respectively, include medium-resolution spectral bands similar to IIR channels.

An assessment of IIR radiances after 9.5 years of nearly continuous operation since launch is presented, thereby updating the first results published in Scott (2009). The paper is organized as follows. A brief description of the IIR instrument is given in Sect. 2. Pre-launch studies for the selection of IIR companion instrument and channels are presented in Sect. 3, and the implementation of the relative and stand-alone approaches is described in Sect. 4. Results and findings from the relative and the stand-alone approaches are presented in Sect. 5 and 6, respectively, and our assessment is summarized in the last section.

2 The IIR/CALIPSO instrument

The whole CALIPSO payload flies in a staring and near nadir looking configuration, with a 0.3° angle from nadir in the forward direction, which was increased to 3° at the end of November 2007 to reduce specular reflections from horizontally oriented ice crystals in CALIOP lidar observations (Hu et al., 2009). The IIR instantaneous field of view is +/- 2.6° or 64x64 km on the ground, with 1-km size pixels. Thus, the viewing angles from nadir range from 0° to 3° until November 2007 and from 1° to 6° after the CALIPSO payload pitch change, which is expected not to have any identifiable impact on the observations.

The IIR instrument (Corlay et al., 2000) includes three filters which are mounted on a rotating wheel for sequential acquisition in the respective spectral bands. The sensor is an uncooled micro-bolometer array (U3000) manufactured by Boeing (also implemented in the IASI instruments). IIR is regularly calibrated in-flight from images of a temperature-monitored warm blackbody source (at about 295 K) and from cold deep space (about 4 K) views. For each spectral band and for each pixel in the image, cold space views are used to determine the off-set of the detection system, and images from the calibration blackbody source of known temperature are used to retrieve the gain. The linearity of the detection system was verified before launch for scene temperatures ranging between 215 K and 320 K, and the gain retrieved from the warm

Atmos. Meas. Tech. Discuss., doi:10.5194/amt-2016-345, 2016
Manuscript under review for journal Atmos. Meas. Tech.
Published: 14 November 2016

calibration source is directly applied to calibrate the earth view images. Instrument Spectral Response Functions (ISRF) for each band were established by CNES before launch and are available upon request.

The overall calibration accuracy of the IIR measurements is specified to be better than 1 K in all channels. In-flight performances were assessed by CNES at the beginning of the mission (Trémas, 2006; Tinto and Trémas, 2008). The in-flight short term gain stability was found better than 0.1 K of equivalent brightness temperature, except during the day-to-night transitions, during which the gain varies by up to 0.45 K. The in-flight noise equivalent differential temperature (NedT) at 210 K was between 0.2 and 0.3 K, similar to values measured before launch, and better than the specified value of 0.5 K. The NedT is of the order of 0.1 K at 250 K.

The calibrated radiances are reported in the CALIPSO Version 1 IIR level 1B products (Vaughan et al., 2015) available at the Atmospheric Science Data Center of the NASA Langley Research Center and at the AERIS/ICARE data center in France. They are re-sampled and registered on a 1-km resolution unique grid centered on the CALIOP lidar ground track, at sea level, with a 69-km swath. The products are organized by separating the daytime and nighttime portions of an orbit to match the definition chosen for the CALIOP lidar instrument, and thereby facilitate synergetic analyses. Because the lidar is very sensitive to daylight background noise, the nighttime portion of the orbit is when the solar elevation angle is less than -5° (Hunt et al., 2009).

3 Method and pre-launch studies

Both the relative and the stand-alone approaches require i) companion instruments that offer the best possible spatio-temporal coincidences with IIR (primarily in order to see the same scenes simultaneously), and ii) companion channels presenting close characteristics in terms of spectral coverage and spatial resolution. These constraints have oriented our choice towards two companion instruments: MODIS/Aqua and SEVIRI/Meteosat.

3.1 Description of companion instruments

MODIS/Aqua and SEVIRI/Meteosat in-flight performances have been extensively characterized (Xiong et al., 2015; EUMETSAT, 2007a and references herein). The main instrumental characteristics of interest for comparison with IIR are summarized in Table 1. They are detailed in the next sub-sections.

3.1.1 MODIS/Aqua

The first companion instrument chosen for this study, MODIS/Aqua, includes three medium resolution spectral bands in the thermal infrared window (29, 31 and 32) with 1-km spatial resolution of interest for comparisons with IIR. Furthermore, both Aqua and CALIPSO, which is nominally positioned 73 s behind Aqua, have been flying in formation with other satellites of the A-Train (Stephens et al., 2002) since June 2006. The A-Train satellites follow a sun-synchronous polar orbit at 705 km altitude with a 98.2° inclination. CALIPSO measurements global coverage is between 82°N and 82°S. There is a

Atmos. Meas. Tech. Discuss., doi:10.5194/amt-2016-345, 2016
Manuscript under review for journal Atmos. Meas. Tech.
Published: 14 November 2016

16-day repetition cycle, with an equator crossing time at about 13:35 local solar time. CALIPSO is controlled according to a customized grid shifted by 7 min 44s local time from the nominal WRS-2 grid used by Aqua, or 215 km eastwards at the equator crossing. Due to the relative positions of the CALIPSO and Aqua satellites in the A-Train, the MODIS 2330-km swath always covers the IIR 69-km swath with nearly simultaneous measurements. The viewing angles for the MODIS pixels collocated with the IIR swath vary with latitude, as illustrated in Fig. 1, which shows histograms of MODIS viewing angles for six 30-degree latitude bands over ocean in July 2014. The MODIS viewing angle is largest at the equator, and ranges from 12° and 20° at 0°-30° latitude in both hemispheres. It decreases progressively as latitude increases, to be mostly between 8° and 18° at 30°-60° north and south, and less than 12° at 60°N-82°N. The pixels over ocean south of 60°S are actually north of about 70°S due the presence of the Antarctic continent, which explains why histograms at 82°S-60°S exhibit larger angles on average than those at 60°N-82°N. These geometries of observation are accounted for in the simulations.

3.1.2 SEVIRI/Meteosat

Comparing IIR and MODIS/Aqua observations, both from the A-Train, ensures a very large sampling for statistical analyses. A complementary view is available through comparisons with SEVIRI on board the geostationary second generation Meteosat satellites. SEVIRI provides radiometric data every 15 minutes in three spectral bands in the thermal infrared (channels IR8.7, IR10.8 and IR12) with a 3-km resolution at the sub-satellite point, which is at 0° in both latitude and longitude. SEVIRI data are from three different prime geostationary satellites since June 2006: Meteosat 8 until 11 April 2007, then Meteosat 9 until 21 January 2013, and finally Meteosat 10 until present. IIR and SEVIRI have been preferably compared when SEVIRI viewing angles are smaller than 10° to be close to IIR quasi-nadir observations, therefore at latitudes between 10°N and 10°S, and longitudes between 10°W and 10°E.

3.2 Selection of IIR, MODIS, and SEVIRI companion channels

The IIR companion channels were chosen before launch among the various spectral channels of MODIS/Aqua and SEVIRI/Meteosat following a specific procedure. For each IIR channel, the selected MODIS or SEVIRI companion channel is the one that not only minimizes the brightness temperature difference (BTD) with IIR, but also shows a similar sensitivity to the atmosphere and to the surface. This evaluation was conducted before launch by simulating the IIR and candidate companion channels using the forward radiative transfer model 4A (4A: Automatized Atmospheric Absorption Atlas) fed by for more than 2300 atmospheres from the TIGR Thermodynamic Initial Guess Retrieval) dataset. MODIS/Aqua ISRFs can be retrieved from the MODIS Characterization Support Team website (http://mcst.gsfc.nasa.gov/calibration/parameters) and SEVIRI/Meteosat ones from the EUMETSAT MSG Calibration website (http://www.eumetsat.int/website/home/Data/Products/Calibration/MSGCalibration/index.html). Due to differences in the spectral position and shape of the ISRFs, and also due to the highly variable land surface emissivity, our study is so far

Atmos. Meas. Tech. Discuss., doi:10.5194/amt-2016-345, 2016
Manuscript under review for journal Atmos. Meas. Tech.
Published: 14 November 2016

Atmospheric Measurement Techniques Discussions

limited to observations over ocean. The simulated BTDs between IIR and the selected companion channels are shown in Sect. 3.2.3, after a brief description of the simulation model and of the auxiliary datasets in Sects. 3.2.1 and 3.2.2.

3.2.1 The forward radiative transfer model: 4A

The radiative transfer model used at all stages of this study is the so-called 4A/OP, the operational version of 4A, adapted and maintained by NOVELTIS (http://4aop.noveltis.com/) in collaboration with CNES and LMD. 4A is a fast and accurate line-by-line (LBL) radiative transfer model initially developed at LMD (Scott and Chédin, 1981). As recalled in Anthony Vincent and Dudhia (2016), 4A was among the pioneer radiative transfer models to bypass LBL processing time by calculating once and for all a set compressed look-up-tables (LUT) of monochromatic optical depths. These LUT are generated by the nominal line-by-line STRANSAC model (Scott, 1974; Tournier et al., 1995) coupled to the GEISA (Gestion et Etude des Informations Spectroscopiques Atmosphériques) spectroscopic database. 4A generates transmittances, radiances, jacobians (Chéruy et al., 1995) for any instrumental, spectral, and geometrical configuration (ground, airborne, satellite).

4A has a long history of validation within the frame of the international radiative transfer community. From the very beginning, most of the validation results have been extensively discussed in a number of intercomparison exercises and in particular during the ITRA (Intercomparison of Transmittance and Radiance Algorithms) working groups - 1983, 1985, 1988, 1991 of the International Radiation Commission (Chédin et al., 1988) and during the ICRCCM (Intercomparison of Radiation Codes in Climate Models) campaigns (Luther et al., 1988). More recently, observations from hyperspectral sounders such as AIRS and IASI have led to even more extensive validations, again within the frame of international observation campaigns or working groups, among them the International Tovs Study Conferences (ITSC) and the IASI Sounding Science Working Group (ISSWG). 4A is the official code selected by CNES for calibration/validation activities of the IASI, Merlin (https://merlin.cnes.fr) and MicroCarb (https://microcarb.cnes.fr) missions. A detailed description of the protocole and of the results of the interactive validation of GEISA and 4A/OP may be found in Armante et al. (2016).

Throughout the 9.5 years of IIR operation analysed here, we have used a frozen version of 4A (2009 version) in order to avoid undesired, however smooth, jumps. The LUT were generated with STRANSAC coupled to the 2011 version of GEISA (Jacquinet-Husson et al., 2011). The 4A/OP model is in “down-up” mode, which means that the emission by the surface, the upwelling atmospheric radiation and the reflection at the surface of the downwelling atmospheric radiation are taken into account, modulated by the emissivity or the reflectivity. A widely accepted mean value of 52 degrees is taken for the computation of the downwelling reflected radiances. Simulations are conducted for relevant MODIS and SEVIRI viewing angles, (see Sect. 3.1 and Fig. 1) and IIR is considered as a nadir viewing instrument. Because the viewing angles are smaller than 20°, no specific dependence of the emissivity on the emission angle has been taken into account. A mean ocean surface emissivity equal to 0.98 for all the channels is taken for these simulations.

Atmos. Meas. Tech. Discuss., doi:10.5194/amt-2016-345, 2016
Manuscript under review for journal Atmos. Meas. Tech.
Published: 14 November 2016

Atmospheric Measurement Techniques Discussions

3.2.2 Atmospheric inputs: the TIGR dataset

The simulations have been conducted for the 2311 atmospheres of the TIGR climatological library (Chédin et al., 1985; Chevallier et al., 1998). Within TIGR, atmospheres are sorted out in five air mass types according to their virtual temperature profiles (Achard, 1991; Chédin et al., 1994), which are namely: 1) *tropical*, 2) *mid-lat1* for temperate conditions, 3) *mid-lat2* for cold temperate and summer polar conditions, 4) *polar1* for very cold polar conditions, 5) *polar2* for winter polar conditions, and which include 872, 388, 354, 104, and 593 atmospheres, respectively.

3.2.3 Brightness temperatures simulations

The 4A model fed by the TIGR atmospheres has been used to simulate the brightness temperatures of IIR and of the candidate companion channels. The mean BTDs between IIR and MODIS or SEVIRI channels and associated standard deviations have been evaluated for the five TIGR air mass types (hereafter "TIGR_BTD"). The simulations presented here have been obtained using the 2009 version of the 4A/OP model presented above, which does not call into question the initial evaluations conducted before the 2006 launch.

The most suitable radiometric pairings of IIR-MODIS channels for our study are IIR1-MODIS29, IIR2-MODIS31, and IIR3-MODIS32. Similarly, the most suitable IIR-SEVIRI pairs are IIR1-SEVIRI8.7, IIR2-SEVIRI10.8, and IIR3-SEVIRI12. Simulations were for SEVIRI/Meteosat 8, which was the primary satellite in June 2006, but our channel selection would be unchanged for the more recent instruments. The ISRFs of these nine channels are plotted in Fig. 2. Brightness temperatures derived from the modeled radiances are computed using the relevant ISRF. As an indication, shown in Table 2 are the equivalent central wavenumbers and wavelengths that minimize the differences between the true temperature and the temperature derived using the Planck function over a range of temperatures stretching from 200 K to 310 K. The central wavenumbers are relevant in case of blackbody radiances expressed in $W/m^2/sr/cm^{-1}$, as in the output of the 4A model, whereas the central wavelengths are relevant in case of radiances reported in $W/m^2/sr/\mu m$, as in the satellite observations. It is noted that the equivalent central wavelengths of IIR1, IIR2, and IIR3 are found to be 8.635 μm, 10.644 μm, and 12.096 μm, respectively.

The TIGR_BTDs between IIR and MODIS companion channels are reported in Table 3 for the five TIGR air mass types. They are given for MODIS viewing angles of 0°, 12°, and 20° chosen according to the latitude-dependent, —and therefore air mass type-dependent, range of viewing angles discussed in Sect. 3.1 and shown in Fig. 1. Variations with the TIGR air mass type reflect the sensitivity to surface temperature, temperature and water vapour profiles, and other absorbing atmospheric constituents. For the three pairs of channels, the absolute TIGR_BTDs and the standard deviations are overall larger for the tropical air mass type than for the other air mass types, related to the high content and high variability of the water vapour in the tropical regions. Except for the tropics, absolute TIGR_BTDs are smaller than 0.2 K for IIR1-MODIS29 and 0.1 K for IIR2-MODIS31, with similar standard deviations smaller than 0.1 K. The largest absolute TIGR_BTDs and

Atmos. Meas. Tech. Discuss., doi:10.5194/amt-2016-345, 2016
Manuscript under review for journal Atmos. Meas. Tech.
Published: 14 November 2016

standard deviations are for the IIR3-MODIS32 pair, with TIGR_BTD of about -1 K and standard deviations up to 0.3 K for tropical air mass types.

TIGR_BTDs between IIR and SEVIRI/Meteosat 8 companion channels for the TIGR tropical air mass and SEVIRI viewing angles equal to 0° and 12° are reported in Table 4. For a 12° viewing angle, IIR-SEVIRI TIGR_BTDs differ by up to 0.5 K from the respective IIR-MODIS TIGR_BTDs.

4. Implementation of the relative and stand-alone approaches

For both the relative and the stand-alone approaches, observations of IIR and its companion channels are first spatially and temporally collocated, as described in the next sub-section. The various steps specific to the implementation of each approach are then detailed.

4.1 Collocations

Collocated observations are from the REMAP product developed, processed and available at the AERIS/ICARE data center. REMAP includes MODIS/Aqua and SEVIRI calibrated radiances collocated with the IIR Level 1B radiances and mapped on the IIR 69-km grid. MODIS calibrated radiances are from MYD021KM Collection 5 with geo-location from MYD03 Collection 5. SEVIRI geo-located and calibrated radiances are from the Level 1.5 Image product, which reports spectral blackbody radiances until 7 May 2008 and effective blackbody radiances afterwards (EUMETSAT, 2007b). For each IIR pixel, the collocated MODIS or SEVIRI radiance is from the closest pixel, at sea level. So far, no spatial averaging of the IIR or MODIS 1-km pixels is performed in order to get a better match with SEVIRI pixels. Thus, one 3-km resolution sub-satellite SEVIRI pixel is collocated with at least nine different IIR pixels, depending on the SEVIRI viewing angle. IIR and MODIS pixels are collocated with the temporally closest SEVIRI image, which is up to 7 min 30 s before or after the companion observation. IIR and MODIS observations are quasi-coincident and are therefore considered always temporally collocated. Overall, IIR and MODIS observations are well collocated, whereas a naturally occurring GEO/LEO “mismatch” between SEVIRI and IIR observations cannot be ignored: spatially - because of the difference in the pixel sizes and the difference in the satellite zenith angles, - nor temporally, because the time difference between the observations can be up to several minutes. The spatial mismatch is minimized by comparing IIR and SEVIRI when SEVIRI viewing angles are less than 10°.

4.2 Relative approach: outputs and statistical analyses

Outputs of the relative approach are here daily means of BTDs and standard deviations. They have been generated for each single day since launch, with daytime and night data either combined or separated, for several 10-K ranges in observed brightness temperatures, from 290-300 K down to 200-210 K.

Atmos. Meas. Tech. Discuss., doi:10.5194/amt-2016-345, 2016
Manuscript under review for journal Atmos. Meas. Tech.
Published: 14 November 2016

Atmospheric Measurement Techniques Discussions

Statistical analyses of BTDs between pairs of channels over ocean are performed for five latitude ranges: in the tropics (30°S-30°N), and at mid- (30°-60°) and polar (60°-82°) latitudes in both hemispheres. Oceanic scenes are identified using an index available from the Global Land One-Kilometer Base Elevation (GLOBE) project (GLOBE Task Team and others, 1999). Thresholds are defined, which are based on the simulated TIGR_BTDs and associated standard deviations (see Tables 3 and 4), and on the expected instrumental NedT (see Table 1). Using TIGR_BTDs corresponding to each latitude band and assuming a standard deviation σ equal to 0.7 K, BTDs larger than TIGR_BTD $\pm$ 3σ (2.1 K) are considered spurious values. The statistics are computed after rejecting the spurious values and performing uniformity tests to ensure the homogeneity of the scenes. Because the collocations are at sea level, these tests should minimize parallax issues in case of elevated clouds.

4.3 Stand-alone approach

4.3.1 Clear sky mask

After collocation of IIR, MODIS, and SEVIRI companion channels (Sect 4.1), a clear sky mask is applied to select the relevant pixels for direct comparisons between observations and simulations. The mask is from the Version 3 IIR Level 2 Swath product (Vaughan et al., 2015). It is derived from collocated IIR and CALIOP observations along the lidar track and extended to the 69-km IIR swath by using radiative homogeneity criteria (Garnier et al., 2012). In the Version 3 of the IIR Level 2 operational algorithm, clear sky track pixels are defined as those pixels for which no cloud layers could be detected by CALIOP, and no depolarizing aerosol layers could be detected after averaging the lidar signal up to 20-km along the track. This information is extracted from the CALIOP Level 2 5-km Cloud and Aerosol Layer products (Vaughan et al., 2015). Initial analyses evidenced that the Version 3 mask is contaminated by the presence of low cloud layers detected by CALIOP at the finest 1/3 km resolution, but not reported in the 5-km layer product, so that they are ignored by the IIR algorithm. This issue will be corrected in the next version 4 of the IIR operational algorithm. Because the new operational product is not available at this time, a corrected mask has been produced specifically for this study. We chose to process each month of January and July from mid-June 2006 to December 2015 to cover the same 9.5-year time period as in the relative approach in two opposite seasons.

4.3.2 Clear sky brightness temperatures simulations

Clear sky simulations of the collocated observations (Sect. 4.1) are carried out using the 4A/OP model (see Sect. 3.2.1) fed by the temporally and spatially closest atmospheric profiles and ocean skin temperatures given by ERA-Interim (ERA-I) reanalyses generated at the European Centre for Medium range Weather Forecast (ECMWF). We have here favoured the use of outputs from reanalyses over outputs based on radiosondes measurements (e.g. the LMD Analyzed RadioSoundings Archive (ARSA) database) because of the low density of the radiosonde network over sea. ERA-I reanalyses are available every 6 hours with a nominal resolution of 0.75° in latitude and longitude. The 4A/OP simulated radiances are computed for each clear pixel found at a distance smaller than 5 km from the closest ERA-I input to ensure the highest possible coherence

Atmos. Meas. Tech. Discuss., doi:10.5194/amt-2016-345, 2016
Manuscript under review for journal Atmos. Meas. Tech.
Published: 14 November 2016

for the comparisons with the observations. This 5 km threshold was chosen taking into account the specificity of each of the three instruments (IIR, MODIS, SEVIRI). The reanalyses outputs give a 61-level description of the temperature, water vapour and ozone profiles as well as the skin temperature. A comprehensive documentation of the current ERA-I reanalysis system used in this study may be found in Dee et al. (2011). For other absorbers with a constant pressure dependent mixing ratio (CO_2, N_2O, CO, HNO_3, SO_2, CFC's, etc), the most plausible mixing ratio value is used.

The MODIS and SEVIRI viewing angles are outputs of the collocation step (Sect. 4.1), and IIR is again considered as a nadir viewing instrument.

Another essential variable for the simulation of the brightness temperatures of these nine window channels is the ocean surface emissivity. As shown for a long time, in a lot of publications, the emissivity depends on wind speed, polarization, temperature, emission angle and wavenumber (Masuda et al., 1988; Wu and Smith, 1996; Brown and Minnett, 1999; Hanafin and Minnett, 2005; Niclòs et al., 2007). In the present study, variations with wind speed or polarization are not taken into account. Indeed, we chose to favour the consistency with the pre-launch simulations so that ocean surface emissivity has been taken equal to 0.98 for all the channels. Again, because MODIS viewing angles are always smaller than 20° and SEVIRI ones are here intentionally limited to 10°, the emissivity dependence on satellite viewing angle is neglected. It is worth pointing out that problems requiring the highest possible absolute accuracy, such as the retrieval of geophysical variables or the validation of radiative transfer models, could not be approached with such approximations. Here, we are more interested in comparing the behaviour of the companion channels for each pair of channels than in comparing the pairs. Because each companion channel of each pair is processed in the same conditions, the relative behaviour would negligibly be affected by this constant value of the emissivity. However, in the planned future reprocessing of the data, and since no limitation comes from the 4A/OP model itself, we plan to detail and take into account all the required dependencies whenever the information is available.

4.3.3 Outputs and statistical analyses

The stand-alone approach generates, for each channel, differences between the 4A simulation and the clear sky observation, hereafter called "residuals". For this study, the 4A simulations have been processed for 10 days of each of the chosen months. Outputs are "monthly" mean residuals and associated standard deviations, with daytime and night data either combined or separated. Statistics are built monthly instead of daily, as done in the relative approach, because the number of items is smaller due to the severe collocation constraints described above. Final statistics are given after removing individual residuals found outside the initial monthly mean ± twice the initial standard deviation. This procedure is to prevent unambiguous outliers to enter the statistics.

Atmos. Meas. Tech. Discuss., doi:10.5194/amt-2016-345, 2016
Manuscript under review for journal Atmos. Meas. Tech.
Published: 14 November 2016

Atmospheric Measurement Techniques Discussions

5 Results and findings from the relative approach

Results from the relative approach are presented hereafter in terms of time series of daily-averaged IIR-MODIS and IIR-SEVIRI BTDs between mid-June 2006 and end December 2015. The findings derived from the analysis of the various figures are then discussed.

5.1 Results

Time series of IIR-MODIS BTDs are shown in Figs 3 to 7 for the five latitude bands, namely 30°S-30°N (Fig. 3), 60°S-30°S (Fig. 4), 30°N-60°N (Fig. 5), 82°S-60°S (Fig. 6) and 60°N-82°N (Fig. 7). Each of these figures includes several panels corresponding to 10-K brightness temperature domains (decreasing from top to bottom) typically found in the respective latitude bands, and each panel shows the brightness temperature differences for the three pairs of channel: IIR1-MODIS29 (red), IIR2-MODIS31 (green), and IIR3-MODIS32 (blue). The mean number of pixels per day used to build the statistics and the mean standard deviations for each pair of channels are shown at the top of each panel and also in Table 5 for more clarity. The mean number of daily pixels is always larger than 5.10^3, and up to $3.7.10^6$ in the tropics at 290-300 K. For each latitude band, the smallest standard deviations are found at the warmest temperatures, with standard deviations ranging from 0.44 K to 0.66 K. Standard deviations increase up to 1.1 K in the tropics at the coldest temperatures, possibly due in part to larger inhomogeneity of cloudy scenes and to parallax effects at larger MODIS viewing angles. Overall, the results show very stable IIR-MODIS BTDs since the CALIPSO launch, with some seasonal variations but with a remarkable year-by-year repeatability. These features will be discussed in more details in Sect. 5.2. It is confirmed that the switch from 0.3° to 3° of the CALIPSO platform pitch angle at the end of November 2007 (see Sect. 2) has no significant impact, because no discontinuity in the time series can be evidenced.

Time series of IIR-SEVIRI BTDs are shown in Fig. 8 for comparison with the IIR-MODIS time series. As explained in Sect. 3.1, SEVIRI viewing angles are chosen smaller than 10°. Consequently, the comparisons are only between about 10°W and 10°E in longitude, and between 10°S and 10°N in latitude. The temperature range is 290-300 K. The mean number of samples per day (5.10^4) is about 100 times smaller than for the IIR-MODIS comparisons. Moreover, the day to day variability is more important and the standard deviations are slightly larger (between 0.49 and 0.65 K). The black and grey arrows point to discontinuities in the time series. The discontinuity of up to 0.4 K in May 2008 (black arrows) is explained by the change of definition in the SEVIRI 1.5 image product from spectral to effective blackbody radiances on 7 May 2008. For simplicity, this change is not accounted for in this analysis, which assumes effective blackbody radiances. This discontinuity was already evidenced in the first analyses reported in Scott (2009). In addition, discontinuities of smaller amplitude (grey arrows) are seen in April 2007, which corresponds to the switch from Meteosat 8 to Meteosat 9, and in January 2013, which coincides with the switch to Meteosat 10. These small discontinuities are explained by the fact that the SEVIRI brightness temperatures are computed using the Meteosat 8 ISRF for the whole period. The discontinuities in the time series illustrate the sensitivity of the technique to detect instrumental changes.

Atmos. Meas. Tech. Discuss., doi:10.5194/amt-2016-345, 2016
Manuscript under review for journal Atmos. Meas. Tech.
Published: 14 November 2016

5.2 Findings

Monitoring differences between IIR and MODIS/Aqua observations, both on the A-Train and with no instrumental changes since CALIPSO launch, appears to be the most fruitful approach for the assessment of the IIR calibration stability since launch. Thus, the findings discussed in the following are based mostly on the IIR-MODIS comparisons shown in Figs. 3 to 7. In this section, we discuss first the consistency of the IIR-MODIS and IIR-SEVIRI BTDs at warm temperature with our pre-launch evaluation from the five TIGR air mass types. Then, we successively discuss the IIR-MODIS results at cold temperature, the long term trends, and the seasonal variations.

5.2.1 Warm scenes

The first step of the analysis is to compare the BTDs from the relative approach with the simulated TIGR_BTDs. Because the TIGR simulations are for clear sky conditions, the comparisons are conducted for the warmest temperature range at each latitude band. Indeed, the clear sky scenes are a priori the warmest ones, although the warmest scenes could also contain clouds of weak absorption or thicker clouds located near the surface. The IIR-MODIS BTDs at the beginning of the mission derived from linear regression lines are reported in Table 6 for comparison against the TIGR_BTDs reported in Table 3. The observed IIR-MODIS BTDs in the tropics at 290-300 K and the TIGR_BTDs for tropical air mass types differ by less than 0.1 K for IIR1-MODIS29, 0.25 K pour IIR2-MODIS31, and 0.3 K for IIR3-MODIS32. The observed mean BTDs at 30°-60° and at 280-290 K in the northern and southern hemispheres and the TIGR_BTDs at mid-latitude (mid-lat1 and mid-lat2) also agree within about 0.1 K for IIR1-MODIS29 and IIR3-MODIS32, and are within 0.2 to 0.3K for IIR2-MODIS31. The same conclusions apply to the mean BTDs at 60°S-82°S and at 270-280 K when compared to the TIGR_BTDs for polar1 and polar 2 atmospheres. At 60°N-82°N, IIR2-MODIS31 and IIR3-MODIS32 BTDS are larger than at 60°S-82°S by about 0.2 K, which degrades the comparisons against the TIGR_BTD. Overall, these results demonstrate the good consistency between observed IIR-MODIS BTDs and simulated TIGR_BTDs, which confirms a posteriori that the thresholds chosen for the relative approach (TIGR_BTD ± 2.1 K) are appropriate and that the statistics are not biased. Direct comparisons between observations and simulations in clear sky conditions will be discussed in Sect. 6 with the stand-alone approach.

Even though the following is based on comparisons against MODIS/Aqua, it is interesting to compare the observed IIR-SEVIRI BTDs and the TIGR_BTDs in the tropics (Table 4). After May 2008, when the radiances reported in the SEVIRI products are effective blackbody radiances, the TIGR_BTDs are in fair agreement with the differences plotted in Fig. 8, keeping in mind that the SEVIRI observations are from Meteosat 9 and 10 after May 2008, whereas the TIGR simulations are for SEVIRI/Meteosat 8.

5.2.2 Cold scenes

As the scene temperature decreases, the mean IIR-MODIS BTDs shown in Figs. 3 to 7 progressively depart from the values found for the warm scenes. For instance, in the tropics (Fig. 3), IIR1-MODIS29 BTD varies from 0.34 K at 290-300 K to 0.7

Atmos. Meas. Tech. Discuss., doi:10.5194/amt-2016-345, 2016
Manuscript under review for journal Atmos. Meas. Tech.
Published: 14 November 2016

Atmospheric Measurement Techniques Discussions

K at 200-210 K, and similarly, IIR2-MODIS31 BTD varies from 0.51 K to 1 K, and IIR3-MODIS32 BTD varies from -0.74 K to -0.2 K. This could be explained by an increasing contribution from absorbing cold clouds and decreasing influence of the surface and near-surface atmosphere to which the IIR and MODIS window channels are the most sensitive for semi-transparent scenes. The coldest temperatures in the tropical and mid-latitude regions correspond *a priori* to elevated dense ice-clouds, which, if they behave as blackbody sources, should lead to quasi-identical brightness temperatures for all channels, assuming a negligible contribution from the atmosphere above the cloud. Thus, IIR3-MODIS32 BTD equal to -0.2 K at 200-210 K seems plausible, but IIR2-MODIS31 equal to 1 K seems too large. Because IIR and MODIS comparisons could be affected by parallax issues for elevated clouds, IIR inter-channel BTDs inherently not submitted to such parallax effects have been analysed. Following the same approach as previously, IIR1-IIR2 (red) and IIR1-IIR3 (green) BTDs computed from linear regression lines are reported in Fig. 9 by temperature range in the tropics (30°S-30°N) and at mid-latitude (60°S-30°S and 30°N-60°N). Again, the variations with temperature are due to the changing influence of absorbing ice and water clouds, related to their optical and microphysical properties. The IIR inter-channels BTDs at 205 K are smaller at mid-latitude (circles and squares) than in the tropics (diamonds), which could be explained by different cloud properties. IIR1-IIR3 BTD is close to 0.1 K at mid-latitude at 205 K, consistent with the fact that the corresponding ice clouds are very dense and can be considered as blackbody sources. However, IIR2-IIR3 BTD tends to 0.6 K/0.8 K in the same conditions. In conclusion, both IIR2-MODIS31 BTD and IIR inter-channel BTDs suggest a possible high bias of IIR2 at 205 K, of about 0.5 K to 0.7 K according to IIR only and of up to 1 K according to IIR2-MODIS31. Importantly, no issue has been identified at warm temperature for IIR2 when compared to MODIS31, which will be confirmed in Sect. 6 using the stand-alone approach. Different performances of the IIR calibration at warm and cold temperatures could be explained by a slight change of the in-flight gain between warm and cold scene temperatures. Nevertheless, because the IIR instrument has only one sensor, observing a specific behaviour at the coldest temperatures for only one channel shows that this explanation is not sufficient. We will continue investigating this question using the detailed description of the cloud vertical structure provided by CALIOP measurements, following the same approach as in the IIR Level 2 algorithm (Garnier et al., 2012).

5.2.3 Long term trends

IIR-MODIS BTDs are very stable year-by-year since mid-June 2006. In order to quantify the trends over the first 9.5 years of the CALIPSO mission, linear regression lines have been computed for each of the time series shown in Figs. 3 to 7. The slopes of these lines well approximate the trend of the IIR-MODIS brightness temperature differences since the beginning of the CALIPSO mission. These trends are plotted against temperature in Fig. 10 for each pair of channels and for each of the five latitude bands. An unambiguous trend is seen for IIR1-MODIS29 (red) at any temperature and at any latitude, varying between -0.01 and -0.03 K/year. It is -0.02 K/year on average. This trend, which represents -0.19 K over the 9.5-year period, can also be seen directly in Figs. 3 to 7. However, the trend of the order of 0.005 K/year or less in absolute value for IIR2-MODIS31 (green) and IIR3-MODIS32 (blue) is deemed not significant. Notwithstanding the small trend evidenced for IIR1-

Atmos. Meas. Tech. Discuss., doi:10.5194/amt-2016-345, 2016
Manuscript under review for journal Atmos. Meas. Tech.
Published: 14 November 2016

MODIS29, which is further investigated in Sect. 6 using the stand-alone approach, the long term stability of the IIR instrument with respect to MODIS/Aqua between June 2006 and end 2015 is remarkable.

5.2.4 Seasonal variations

Seasonal variations of the IIR-MODIS BTDs are sometimes observed at mid- and high latitude in Figs. 4 to 7. More specifically, it can be noted by comparing Figs. 4 and 5 on one hand (mid-latitudes) and Figs. 6 and 7 on the other hand (polar latitudes) that for the warmest temperatures, with smallest influence from clouds, a seasonal variability is clearly seen in the northern hemisphere but barely in the southern hemisphere. This phenomenon could be partly explained by the more pronounced seasonal variations of the atmospheric and surface properties in the northern than in the southern latitude bands. However, it was found that at mid-latitudes, where observations during both daytime and nighttime are available year-round, the larger seasonal variability is related to significant differences between nighttime and daytime IIR-MODIS BTDs. This is illustrated in Figs 11 and 12, where the IIR-MODIS BTDs are shown for each pair of channels at 30°N-60°N (Fig. 11) and at 60°S-30°S (Fig. 12), at 280-290 K, and by distinguishing daytime data (in red) from nighttime data (in blue). The BTDs obtained by combining daytime and nighttime data, as in Figs 4 and 5, are plotted in black for reference. At 30°N-60°N (Fig. 11), seasonal night/day biases are seen for the three pairs of IIR-MODIS channels, whereas no night/day biases are seen in the southern hemisphere at 60°S-30°S (Fig. 12). The largest bias at 30°N-60°N is during June/July, with a night-minus-day difference equal to +0.4 K for IIR2-MODIS31 (middle) and IIR3-MODIS32 (bottom), and equal to about 0.2 K for IIR1-MODIS29 (top). In the opposite season, no night/day bias is seen for IIR1-MODIS29, whereas the night-day difference is about -0.1 K for the other pairs. This behaviour is further discussed in Sect. 6 after the presentation of additional information from the stand-alone approach.

6 Results and further findings from the stand-alone approach

The stand-alone approach has been applied to each of the three IIR channels and each of their three MODIS and SEVIRI companion channels to directly compare clear sky simulations and clear sky measurements. Here, results are shown for IIR and MODIS only, for each month of January and July from mid-2006 to end 2015, with the corrected clear sky mask processed as in Sect. 4.3.1. From the relative approach (Sect. 5.2.3), a trend of -0.02 K/year on average is detected for IIR1-MODIS29, which could originate from one channel or from both. The stand-alone approach allows asserting which channel deviates from the other. Similarly, the night/day biases evidenced for each pair of channels in the northern hemisphere at 30°-60° (Sect. 5.2.4) are investigated.

6.1 Results

The fraction of clear sky IIR pixels over ocean is the largest in the tropics at 30°S-30°N, with 20% of the ocean pixels on average nighttime, and 25% daytime. The slightly larger daytime fraction could be in part due to the smaller signal to noise

Atmos. Meas. Tech. Discuss., doi:10.5194/amt-2016-345, 2016
Manuscript under review for journal Atmos. Meas. Tech.
Published: 14 November 2016

ratio of the lidar signal, and therefore to a reduced ability to detect clouds. Fig. 13 shows the mean monthly residuals obtained over ocean in the tropics for IIR1 and MODIS29 (top), IIR2 and MODIS31 (middle), and IIR3 and MODIS32 (bottom), night and day. Each monthly value is obtained from typically 4.10^3 simulations. Linear regression lines with temporal origin at the beginning of the mission are also plotted, with slopes and intercepts given on each panel. The residuals are found between 0.2 K and 0.6 K, which is deemed reasonable keeping in mind that they are sensitive to the auxiliary data (including the clear sky mask) and that the surface emissivity is taken constant and equal to 0.98 for all channels. The standard deviations are found between 0.4 and 0.6 K for the IIR channels, and between 0.5 and 0.7 K for the MODIS channels. Values from IIR and MODIS are comparable, showing the importance of uncertainties in ancillary inputs as compared to the instrumental noise. Using the Version 3 non-corrected IIR clear sky mask leads to significantly larger standard deviations, up to 1.2 K. Moreover, these residuals are larger by about 0.5 K, with season- and latitude- dependent biases, which is fully consistent with the presence of unwanted cloudy and therefore too cold observations in these supposedly "clear sky" data samples.

IIR1 (0.412 K) and MODIS29 (0.392 K) residuals shown in Fig. 13 differ by only 0.02 K at the beginning of the mission, and IIR2 (0.208 K) and MODIS31 (0.249 K) residuals differ by only 0.04 K. This indicates that for these pairs, the differences between the observations are well reproduced by the simulations, suggesting an excellent accuracy of the IIR calibration. However, the IIR3 residuals (0.324 K) are smaller than the MODIS32 residuals (0.579 K) by -0.26 K. Because residuals are differences between simulations and observations, this means that the simulated IIR3-MODIS32 differences are smaller than the observed differences by -0.26 K.

6.2 Further findings

6.2.1 IIR1-MODIS29 trend

Similar temporal variations of the monthly residuals in Fig. 13, of the order of or less than 0.1 K, are seen for all the channels of the two instruments, indicating that they originate from the simulations rather than from the observations. The slope of the MODIS29 residuals, -0.019 K/year, is much larger than that of IIR1, 0.0017 K/year, meaning that MODIS29 observations have increased with respect to the simulations at a rate of +0.019 K/year, whereas IIR1 ones have barely changed. This is in good agreement with the decrease of IIR1-MODIS29 BTDs at a rate of -0.02 K/year seen in the relative approach. For the IIR2-MODIS31 and IIR3-MODIS32 pairs, the absence of detectable trend in the relative approach suggests that none of these four channels has been drifting. As expected, the slopes of the four residuals are quasi-identical and do not exceed -0.0037 K/year. Overall, this indicates that the much larger slope of the MODIS29 residuals is driven by MODIS observations and not by the simulations. In conclusion, none of the IIR channel exhibits a detectable trend, whereas MODIS29 exhibits a positive trend of about +0.019 K/year since the beginning of the CALIPSO mission. It is recalled that MODIS Collection 5 products are used for this analysis, so that this assessment may not be applicable to the most recent Collection 6.

Atmos. Meas. Tech. Discuss., doi:10.5194/amt-2016-345, 2016
Manuscript under review for journal Atmos. Meas. Tech.
Published: 14 November 2016

Atmospheric Measurement Techniques Discussions

6.2.2 IIR-MODIS night/day bias at 30°N-60°N

A night/day bias has been evidenced for each pair of IIR-MODIS observations in the northern hemisphere at 30°-60°, which varies seasonally and has its maximum amplitude in June/July (see Sect. 5.2.4 and Fig. 11). For further assessment, Fig. 14 shows the IIR and MODIS residuals for the three pairs of channels against latitude for the month of July 2007 by separating nighttime (top) and daytime (bottom) clear sky observations. Again, the results have to be interpreted in a relative sense. At night (top) and south of 25°N, the IIR1 and MODIS29 residuals (red curves) and the IIR3 and MODIS32 residuals (blue curves) exhibit quasi-identical latitudinal variations, which are therefore attributed to the simulations. IIR2 and MODIS31 residuals (green curves) are very close from 35°S to 25°N, and slightly depart from each other by up to 0.2 K south of 35°S. Similar results are obtained during daytime (bottom) south of 25°N. At night, from 25°N to 45°N, the three MODIS residuals (open circles) and the IIR1 residuals (red, full circle) have similar latitudinal variations, whereas IIR2 (green, full circle) and IIR3 (blue, full circle) residuals unambiguously decrease more rapidly than the others, by about 0.5 K. However, during daytime, no distinct behaviour of the IIR2 and IIR3 residuals is seen between 25°N and 45°N. The sudden decrease from 25°N to 45°N seen for the IIR2 (respectively IIR3) nighttime residual, but not for the residual of its companion channel MODIS31 (respectively MODIS 32), indicates that this phenomenon originates from the observations. Furthermore, the fact that this sudden decrease is seen only for the IIR2 and IIR3 residuals and is seen at night but not during the day strongly suggests a calibration bias in IIR2 and IIR3 observations at night. A sudden decrease of the residuals means a sudden increase of the IIR2 and IIR3 brightness temperatures, by up to 0.5 K from about 30°N to 45°N. Thus, the stand-alone approach shows that the night-minus-day differences of +0.4 K seen for IIR2-MODIS31 and IIR3-MODIS31 in June/July in the northern hemisphere at 30°-60° (Fig. 11) using the relative approach are due to the fact that IIR2 and IIR3 channels are biased and too warm at night. It is recognized that the smaller night-day differences seen for IIR1-MODIS29 (+0.2 K) in Fig. 11 is not clearly evidenced from the stand-alone approach. No issue is evidenced in the southern hemisphere and south of 25°N from the stand-alone approach, which is consistent with the fact that nighttime and daytime IIR-MODIS BTDs at 60°-30° in the southern hemisphere are nearly identical (Fig. 12).

It is noted that south of 25°N, all nighttime residuals tend to be larger than daytime ones, by about 0.2 K. However, differences due to the clear sky mask are expected to lead to larger daytime residuals because of the a priori larger probability for the lidar to miss clouds during daytime. Thus, even though the clear sky mask may partly explain these differences, it is likely not the only contributor. Nevertheless, these small differences do not impact the previous discussion.

The IIR calibration biases evidenced at mid-latitude in the northern hemisphere are being investigated in collaboration with CNES. Our current understanding is that the rapidly changing thermal environment of the instrument at the end of the daytime portion and at the beginning of the nighttime portion of the orbits in the northern hemisphere would not be perfectly accounted for through the blackbody source used for the in-flight calibration. The flaw is synchronized with the elapsed time since the night-to-day transition along the orbit. Because the latitude of the night-to-day transition depends on the season, the flaw appears at season-dependent latitudes, but always in the northern hemisphere (T. Trémas, private communication),

Atmos. Meas. Tech. Discuss., doi:10.5194/amt-2016-345, 2016
Manuscript under review for journal Atmos. Meas. Tech.
Published: 14 November 2016

which in turn explains the observed seasonal variations at fixed latitudes (30°N-60°N). These calibration biases are expected to impact the IIR1-IIR3 inter-channel BTD by less than 0.2 K on average, and to have no significant impact on IIR2-IIR3 on average.

7 Summary and conclusions

An assessment of the IIR calibration after 9.5 years of nearly continuous operation has been presented. IIR channels IIR1 (08.65 μm), IIR2 (10.6 μm), and IIR3 (12.05 μm) have been primarily compared against MODIS/Aqua Collection 5 companion channels MODIS29, MODIS31, and MODIS32, respectively, both on the A-Train with no instrumental changes since the CALIPSO launch. The choice of the companion instruments and channels was based on criteria such as spectral range and BTDs between IIR and the candidate channels, quality and frequency of the spatial and temporal coincidences with the IIR 69-km swath, and spatial resolution. BTDs between IIR and companion channels have been evaluated before launch using the 4A radiative transfer model and five air mass types determined from the TIGR climatic data base (TIGR_BTD, Table 3). The simulation, collocation and statistical tools have been developed to perform also comparisons with SEVIRI companion channels SEVIRI8.7, SEVIRI10.8, and SEVIRI12.

Two complementary approaches have been applied, which aim at characterizing deviations between the pairs of companion channels as well as the behaviour of each individual channel both qualitatively and quantitatively. The relative approach is based on statistical analyses of BTDs between IIR and the relevant companion channels in controlled conditions, over a wide range of brightness temperatures, and over ocean. This approach uses only calibrated and geo-located radiances, and does not require additional information from the lidar, such as the clear sky mask. The stand-alone approach is based on direct comparisons between simulations and observations (residuals) in clear sky conditions, using the 4A/OP model fed by time-space collocated ERA-Interim reanalysis products. The clear sky mask is derived from the Version 3 IIR Level 2 Swath product, and has been corrected for this study to account for additional clouds detected by CALIOP at 1/3 km resolution but not accounted for in the current IIR operational algorithm. Overall, a remarkable stability of IIR with respect to MODIS companion channels is seen in the southern hemisphere and in the tropics since launch using the relative approach. No long term trend could be detected for the IIR channels, MODIS31, and MODIS32. However, a trend of -0.02 K/year on average is seen for IIR1-MODIS29 at any latitude. The complementary stand-alone approach showed that it originates from a long term positive trend of MODIS29. A seasonal and systematic night IIR calibration bias has been evidenced at mid-latitude in the northern hemisphere. It was first detected with the relative approach through surprising differences between night and daytime IIR-MODIS BTDs, and was further assessed by comparing latitudinal variations of MODIS and IIR residuals of the stand-alone approach for the month of July 2007. The worst bias at 30°N-60°N is in June/July, where IIR2 and IIR3 night brightness temperatures are on average too large by 0.4 K, and IIR1 ones are too large by 0.2 K. IIR calibration with respect to MODIS has been assessed by comparing the residuals of the stand-alone approach for each pair of companion channels. In the tropics, IIR1 and MODIS29 residuals differ by less than 0.02 K, and IIR2 and MODIS31 ones are within 0.04 K.

However, IIR3-MODIS32 BTD is larger than simulated by 0.26 K. This is deemed again a remarkable agreement when compared to the specifications for the IIR instrument (accuracy better than 1 K). Unfortunately, the assessment at very cold temperatures is more uncertain without the support of simulations. The analysis suggests that IIR2 may be biased high by 0.5 to 1 K at 205 K, but this is not evidenced by the stand-alone approach at warmer temperatures. We will continue investigating this issue.

Overall, IIR on-orbit calibration over 9.5 years is excellent and very stable in the southern hemisphere and in the tropics, well within specifications, with no sign of instrumental aging. Corrections for the residual biases identified in the northern hemisphere are being developed in collaboration with CNES for implementation in a future version of the IIR Level 1B products. The monitoring of the IIR instrument will be continued in collaboration with AERIS/ICARE and will be updated as new versions of the IIR products become available. The stand-alone approach will be completed for every month since CALIPSO launch using the corrected mask, which will be implemented in the next version 4 of the IIR Level 2 products. The clear sky simulations will be refined by using more accurate estimates of ocean surface emissivity.

It is believed that this assessment reinforces the value of the collocated IIR and CALIOP data record from the CALIPSO mission, which has now reached 10 years in orbit as part of the A-Train. This work is part of the efforts made in the international research community and space agencies (approximately 15 contributors in GSICS for these latter ones) to provide improved and consistent level 1 and level 2 products from various space-borne instruments for atmospheric science or climate monitoring.

Acknowledgements

The authors are deeply grateful to CNES, NASA Langley Research Center, and SSAI for their support. This work benefited from the support of Centre National de la Recherche Scientifique (CNRS) and of Institut National des Sciences de l'Univers (INSU).

Numerous people have contributed to this work over the years. The experience gained at the occasion of the NOAA/NASA Pathfinder Program and related research since then have paved the way to this study: warmest thanks go to Alain Chédin and colleagues from LMD for stimulating discussions at all the stages of this work. We are thankful to Thérèse Barroso and Pascale Ferrage, former and current CNES CALIPSO mission coordinators, for helpful discussions about the IIR instrument, and to Patricia Lucker (SSAI) for her encouragements. We thank Jacques Descloitres, Jean-Marc Nicolas, and Fabrice Ducos from AERIS/ICARE for their assistance and Olivier Chomette (LMD) for his contribution at the early stage of this work.

We are thankful to Didier Renaut, Denis Blumstein and Denis Jouglet from CNES for giving us the opportunity to present our results at the occasion of GSICS Meetings.

CALIPSO data are processed and available at the NASA Langley Research Center, and are also available at the AERIS/ICARE data center. The REMAP product is processed and available at AERIS/ICARE. For the post-processing of the satellite data and for the archiving, we also benefited from the large facilities of the Institute for Development and

Resources in Intensive Scientific computing (IDRIS) of CNRS and of the Ensemble de Services Pour la Recherche à l'IPSL (ESPRI)/AERIS data and computing center at IPSL.

References

Achard, V. : Trois problèmes de l'analyse 3D de la structure thermodynamique de l'atmosphère par satellite : mesure du contenu en ozone ; classification des masses d'air ; modélisation 'hyper-rapide' du transfert radiatif, Thèse de doctorat en Terre, océan, espace, Paris 7 University, Paris, 1991.

Anthony Vincent, R. and Dudhia, A.: Fast radiative transfer using monochromatic look-up tables, J Quant. Spectrosc. Radiat. Transfer, http://dx.doi.org/10.1016/j.jqsrt.2016.04.011, 2016.

Armante, A., Scott, N. A., Crevoisier, C., Capelle, V., Crépeau, L., Jacquinet, N., and Chédin, A.: Evaluation of spectroscopic databases through radiative transfer simulations compared to observations. Application to the validation of GEISA 2015 with IASI and TCCON. J. of Mol. Spectr., 327, 180–192, http://dx.doi.org/10.1016/j.jms.2016.04.004, 2016.

Bériot, N., Scott, N. A, Chédin, A., and Sitbon, P.: Calibration of geostationary-satellite infrared radiometers using the Tiros-N vertical sounder: application to Meteosat-1, J. Appl. Meteor., 21, n° 1, 84-89, http://dx.doi.org/10.1175/1520-0450(1982)021<0084:COGSIR>2.0.CO;2, 1982.

Brown, O. B. and Minnett, P. J.: MODIS infrared sea surface temperature algorithm – Algorithm Theoretical Basis Document. Products: MOD28. ATBD Reference Number: ATBD-MOD-25, 1999.

Chédin, A., Scott, N. A., Wahiche, C., and Moulinier, P.: The improved initialization inversion method: a high-resolution physical method for temperature retrievals from satellites of the TIROS-N series, J. Clim. and Applied Meteor., 24, 128-143, 1985.

Chédin, A., and Coauthors: ITRA (Intercomparison of Transmittance and Radiance Algorithms) campaigns and workshops. A report of the International Radiation Commission Joint Meeting ITRA- ICRCCM, University of Maryland, March 1986, 1988.

Chédin, A., Scott, N. A., Claud, C., Bonnet, B., Escobar-Munoz, J., Dardaillon, S., Cheruy, F., and Husson, N.: Global scale observation of the Earth for climate studies, Adv. Space Research, 14, n° 1, 155-159, doi:10.1016/0273-1177(94)90364-6, 1994.

Chéruy, F., Scott, N. A., Armante, R., Tournier, B., and Chédin, A.: Contribution to the development of radiative transfer models for high spectral resolution observations in the infrared, J. Quant. Spectrosc. Radiat. Transfer, 53, 597-611, 1995.

Chevallier, F., Chéruy, F., Scott, N. A., and Chédin, A.: A neural network approach for a fast and accurate computation of longwave radiative budget, J. Appl. Meteor., 37:11, 1385-1397, 1998.

Corlay, G., Arnolfo, M.-C. Bret-Dibat, T., Lifermann, A., and Pelon, J.: The Infrared Imaging Radiometer for PICASSO-CENA., CNES Tech. Doc., 14 pp., available online at

https://calipso.cnes.fr/sites/default/files/migration/smsc/calipso/IIR_ICSO00_S2-06.pdf, (last access 13 October 2016), 2000.

Dee, D. P., and Coauthors: The ERA-Interim reanalysis: configuration and performance of the data assimilation system, Q.J.R. Meteorol. Soc., 137, 553–597. doi:10.1002/qj.828, 2011.

EUMETSAT: Typical radiometric accuracy and noise for MSG–1/2, *Rep. EUM/OPS/TEN/07/0314*, 4 pp., Darmstadt, Germany, 2007a.

EUMETSAT: A planned change to the MSG Level 1.5 image product radiance definition, *Rep. EUM/OPS-MSG/TEN/06/0519 issue v1A*, 9 pp., Darmstadt, Germany, 2007b.

Garnier A., Pelon, J., Dubuisson, P., Faivre, M., Chomette, O., Pascal, N., and Kratz, D. P.: Retrieval of cloud properties using CALIPSO Imaging Infrared Radiometer. Part I: effective emissivity and optical depth, J. Appl. Meteor. Climatol., 51, 1407-1425, doi:10.1175/JAMC-D-11-0220.1, 2012.

Garnier, A., Pelon, J., Dubuisson, P.,Yang, P., Faivre, M., Chomette, O., Pascal, N., Lucker, P., and Murray, T.: Retrieval of cloud properties using CALIPSO Imaging Infrared Radiometer. Part II: effective diameter and ice water path, J. Appl. Meteor. Climatol., 52, 2582-2599, doi:10.1175/JAMC-D-12-0328.1, 2013.

GLOBE Task Team, and others: The Global Land One-kilometer Base Elevation (GLOBE) Digital Elevation Model, Version 1.0, National Oceanic and Atmospheric Administration, National Geophysical Data Center, 325 Broadway, Boulder, Colorado 80305-3328, U.S.A. Digital data base on the World Wide Web (URL: http://www.ngdc.noaa.gov/mgg/topo/globe.html) and CD-ROMs, eds. 1999.

Goldberg, M., and Coauthors: The global space-based inter-calibration system (GSICS), Bull. Amer. Meteor. Soc., vol. 92, n° 4, 468–475, 2011.

GSICS Global Space-based Inter-Calibration System: Vision of GSICS in the 2020s: shaping GSICS to meet future challenges, WMO/GSICS-RD002 v1.1, 12 pp., 2015.

Hanafin, J. A. and Minnett, P. J.: Measurements of the infrared emissivity of a wind-roughened sea surface, Appl. Opt., 44, 398-411, 2005.

Hu, Y., Winker, D., Vaughan, M., Lin, B., Omar, A., Trepte, C., Flittner, D., Yang, P., Sun, W., Liu, Z., Wang, Z., Young, S., Stamnes, K., Huang, J., Kuehn, R., Baum, B., and Holz, R.: CALIPSO/CALIOP Cloud Phase Discrimination Algorithm, J. Atmos. Oceanic Technol., 26, 2293-2309, doi:10.1175/2009JTECHA1280.1, 2009.

Hunt, W., Winker, D., Vaughan, M., Powell, K., Lucker, P., and Weimer, C.: CALIPSO lidar description and performance assessment, J. Atmos. Oceanic Technol., 26**,** 1214–1228, 2009.

Jacquinet-Husson N., L., and Coauthors: The 2009 edition of the GEISA spectroscopic database, J. Quant. Spectrosc. Radiat. Transfer, 112, 2395-2445 doi:10.1016/j.jqsrt.2011.06.004, 2011.

Jouglet, D., and Coauthors: Short performance status of IASI on MetOp-A and MetOp-B, Radiometric and spectral inter-comparison of IASI; Validation of Level1c at LMD : An interactive intercalibration and stand-alone approaches for IASI

on board MetopA and MetopB and IIR on board CALIPSO**,** GSICS meeting, 24-28 March 2014, EUMETSAT, Darmstadt, 2014.

Luther, F. M., Ellingson, R. G., Fouquart, Y., Fels, S., Scott, N. A., and Wiscombe, W.: Intercomparison of Radiation Codes in Climate Models (ICRCCM): longwave clear sky results, Bull. Amer. Meteor. Soc., 69, 40-48, 1988.

Masuda K., Takashima, T., and Takayama, Y.: Emissivity of pure and sea waters for the model sea surface in the infrared window regions, Remote Sens. Environ., 24, 313–329, 1988.

Niclòs, R., Caselles, V., Coll, C., and Valor, E.: Determination of sea surface temperature at large observation angles using an angular and emissivity dependent split-window equation, Remote Sens. Environ., 111, 107-121, 2007.

Scott, N. A.: A direct method of computation of transmission function of an inhomogeneous gaseous medium: description of the method and influence of various factors, J. Quant. Spectrosc. Radiat. Transfer, 14, 691-707, 1974.

Scott, N.: Assessing CALIPSO IIR radiance accuracy via stand-alone validation and a GEO/LEO inter-calibration approach using MODIS/Aqua and SEVIRI/MSG, GSICS Quarterly, 3, No. 3, available at http://www.star.nesdis.noaa.gov/smcd/GCC/documents/newsletter/GSICS_Quarterly_Vol3No3_2009.pdf, (last access 8 July 2016), 2009.

Scott, N. A. and Chedin, A.: A fast line-by-line method for atmospheric absorption computations: The Automatized Atmospheric Absorption Atlas, J. Appl. Meteor., 20, 802-812, 1981.

Scott, N. A., Chédin, A., Armante, R., Francis, J., Stubenrauch, C., Chaboureau, J.-P., Chevallier, F., Claud, C., and Chéruy, F.: Characteristics of the TOVS Pathfinder Path-B data set, Bull. Amer. Meteor. Soc., 80, 2679-2701, 1999.

Stephens, G. L., and Coauthors: The CloudSat mission and the A-Train: A new dimension of space-based observations of clouds and precipitation, Bull. Amer. Meteor. Soc., 83, 1771–1790, 2002.

Tinto, F. and Trémas, T.: IIR Level 1 Status, 2nd CALIPSO Exploitation Review, Norfolk (VA), USA, 2008.

Tournier, B., Armante, R., and Scott, N. A. : STRANSAC-93 et 4A-93: Développement et validation des nouvelles versions des codes de transfert radiatif pour application au projet IASI, Internal Rep. LMD, No. 201, LMD/CNRS, Ecole Polytechnique, Palaiseau, France, 1995.

Trémas, T.: Rapport de recette en vol – Radiométrie IIR-Calipso, CNES Tech. Doc CAL-IIR-RP-1189-CNES, 30 pp., Toulouse, France, 2006.

Vaughan, M., Pitts, M., Trepte, C., Winker, D., Detweiler, P., Garnier, A., Getzewitch, B., Hunt, W., Lambeth, J., Lee, K.-P , Lucker, P., Murray, T., Rodier, S., Trémas, T., Bazureau, A., and Pelon, J.: CALIPSO data management system data products catalog, document No. PC-SCI-503, Release 3.8, available online at http://www-calipso.larc.nasa.gov/products/CALIPSO_DPC_Rev3x8.pdf (last access: 13 October 2016), 2015.

Winker, D. M., and Coauthors: The CALIPSO mission: A global 3D view of aerosols and clouds, Bull. Amer. Meteor. Soc., 91, 1211-1229, doi:10.1175/2010BAMS3009.1, 2010.

Wu, X. and Smith, W. L.: Sensitivity of sea surface temperature retrieval to sea surface emissivity, Acta Meteor. Sinica, 10, 376-384, 1996.

Xiong, X., Wu, A., Wenny, B. N., Madhavan, S., Wang, Z., Li, Y., Chen, N., Barnes, W. L., and Salomonson, V. V.: Terra and Aqua MODIS thermal emissive bands on-orbit calibration and performance, IEEE Transactions on Geoscience and Remote Sensing, 53, 5709-5721, doi: 10.1109/TGRS.2015.2428198, 2015.

Atmos. Meas. Tech. Discuss., doi:10.5194/amt-2016-345, 2016
Manuscript under review for journal Atmos. Meas. Tech.
Published: 14 November 2016

Atmospheric Measurement Techniques Discussions

1 **Table 1: Main characteristics of the instruments and channels considered for this study.**

2

Instrument	IIR	MODIS	SEVIRI
Platform	CALIPSO	AQUA	Meteosat 8, 9, and 10
Orbit	LEO, A-Train 73 s behind AQUA	LEO, A-Train	GEO
Temporal coverage	Sun-synchr. 13:43 16-day repetition	Sun-synchr. 13:35 16-day repetition	15 min repeat cycle
Geographical coverage for the study	From WRS-2 grid Lat.: 82°S - 82° N All longitudes	WRS-2 grid Lat. : 82°S - 82°N All longitudes	Lat : 10°S-10°N Long : 10°W - 10°E
Spectral bands	#1: 8.2-9.05 µm #2: 10.35-10.95 µm #3: 11.6-12.6 µm	#29: 8.4-8.7 µm #31: 10.78-11.28 µm #32: 11.77-12.27 µm	IR8.7: 8.3 - 9.1 µm IR10.8: 9.8 - 11.8 µm IR12: 11.0 - 13.0 µm
Swath	69 km	2330 km	Full disk
Resolution	1 km	1 km	3 km sub-satellite
NedT	0.2 - 0.3 K @ 210K 0.1 K @ 250 K	< 0.025 K (Xiong et al., 2015)	< 0.12 K (EUMETSAT, 2007a)

3

Atmos. Meas. Tech. Discuss., doi:10.5194/amt-2016-345, 2016
Manuscript under review for journal Atmos. Meas. Tech.
Published: 14 November 2016

Atmospheric Measurement Techniques Discussions

1 **Table 2: Equivalent central wavelengths and wavenumbers.**

2

	Channel/wavelength/ wavenumber	Channel/wavelength/ wavenumber	Channel/wavelength/ wavenumber
IIR	#1: 8.635 μm 1158.4 cm^{-1}	#2: 10.644 μm 939.9 cm^{-1}	#3: 12.096 μm 829.1 cm^{-1}
MODIS Aqua	#29: 8.553 μm 1169.3 cm^{-1}	#31:11.025 μm 907.6 cm^{-1}	#32: 12.044 μm 830.8 cm^{-1}
SEVIRI Meteosat 8	IR8.7: 8.706 μm 1148.7 cm^{-1}	IR10.8: 10.773 μm 929.3 cm^{-1}	IR12: 11.951 μm 838.7 cm^{-1}

3

Atmos. Meas. Tech. Discuss., doi:10.5194/amt-2016-345, 2016
Manuscript under review for journal Atmos. Meas. Tech.
Published: 14 November 2016

Atmospheric Measurement Techniques Discussions

Table 3: Simulated brightness temperature difference (TIGR_BTD) in Kelvin between IIR and MODIS/Aqua companion channels for MODIS viewing angles of 0°, 12°, and 20°, whenever relevant (NA if not), and standard deviation (in italic) for five air mass types from the TIGR data base.

TIGR		IIR1- MODIS29	IIR2- MODIS31	IIR3- MODIS32
Airmass	Nb. Atm.	0°/12°/20°/*std dev*	0°/12°/20°/*std dev*	0°/12°/20°/*std dev*
tropical	872	NA/0.23/0.37/*0.13*	NA/0.27/0.37/*0.33*	NA/-1.02/-0.89/*0.28*
mid-lat1	388	0.05/0.09/0.17/*0.07*	0.02/0.04/0.07/*0.06*	-0.54/-0.52/-0.49/*0.29*
mid-lat2	354	0.04/0.08/0.14/*0.06*	-0.01/-0.00/0.02/*0.02*	-0.41/-0.39/-0.37/*0.19*
polar1	104	0.0/-0.00/NA/*0.04*	-0.01/-0.00/NA/*0.03*	-0.13/-0.13/NA/*0.15*
polar 2	593	-0.01/0.03/NA/*0.06*	0.03/0.03/NA/*0.03*	-0.15/-0.15/NA/*0.15*

Atmos. Meas. Tech. Discuss., doi:10.5194/amt-2016-345, 2016
Manuscript under review for journal Atmos. Meas. Tech.
Published: 14 November 2016

Atmospheric Measurement Techniques Discussions

Table 4: Simulated brightness temperature difference (TIGR_BTD) in Kelvin between IIR and SEVIRI/Meteosat 8 companion channels for SEVIRI viewing angles of 0° and 12°, and standard deviation (in italic) for the tropical air mass type from the TIGR data base.

TIGR Airmass	IIR1- SEVIRI8.7 0°/12°/*std dev*	IIR2- SEVIRI10.8 0°/12°/*std dev*	IIR3- SEVIRI12 0°/12°/*std dev*
tropical	-0.35/-0.28/*0.21*	0.06/0.12/*0.1*	-0.77/-0.70/*0.25*

Atmos. Meas. Tech. Discuss., doi:10.5194/amt-2016-345, 2016
Manuscript under review for journal Atmos. Meas. Tech.
Published: 14 November 2016

Atmospheric Measurement Techniques Discussions

Table 5: Mean number of pixels per day (bold) and mean standard deviations in Kelvin (from left to right: x=IIR1-MODIS29, y=IIR2-MODIS31, and z=IIR3-MODIS32) associated to Figs. 3 to 7.

	30°S-30°N (Fig. 3) **Pixels** x/y/z	60°S-30°S (Fig. 4) **Pixels** x/y/z	30°N-60°N (Fig. 5) **Pixels** x/y/z	82°S-60°S (Fig. 6) **Pixels** x/y/z	60°N-82°N (Fig. 7) **Pixels** x/y/z
290-300 K	**3.7 10^6** 0.48/0.63/0.48	/	/	/	/
280-290 K	**2.1 10^6** 0.83/0.88/0.84	**1. 10^6** 0.56/0.66/0.63	**6.8 10^5** 0.57/0.66/0.64	/	/
270-280 K	**5.4 10^5** 0.87/0.95/0.94	**1.5 10^6** 0.68/0.73/0.71	**6.8 10^5** 0.69/0.77/0.74	**5.9 10^4** 0.44/0.52/0.5	**4.1 10^5** 0.55/0.62/0.61
260-270 K	**1.7 10^5** 1.1/1.1/1.1	**1.1 10^6** 0.77/0.82/0.79	**4.3 10^5** 0.84/0.89/0.87	**6.0 10^5** 0.61/0.68/0.64	**8.4 10^5** 0.66/0.72/0.70
250-260 K	**1.1 10^5** 1.1/1.1/1.1	**6.9 10^5** 0.82/0.87/0.85	**2.7 10^5** 0.90/0.94/0.93	**1.0 10^6** 0.61/0.67/0.63	**9.1 10^5** 0.68/0.71/0.70
240-250 K	**7.9 10^4** 1.1/1.1/1.2	**3.8 10^5** 0.89/0.90/0.90	**1.4 10^5** 0.97/0.98/0.98	**8.1 10^5** 0.62/0.69/0.65	**6.6 10^5** 0.72/0.75/0.75
230-240 K	**6.6 10^4** 1.1/1.1/1.2	**1.8 10^5** 0.91/0.92/0.93	**7.8 10^4** 0.97/0.98/0.98	**2.6 10^5** 0.65/0.72/0.71	**1.7 10^5** 0.80/0.81/0.81
220-230 K	**5.7 10^4** 1.1/1.1/1.1	**5.8 10^4** 0.94/0.94/0.94	**2.9 10^4** 0.99/0.99/0.99	**9.8 10^4** 0.67/0.71/0.71	**1.3 10^4** 0.87/0.87/0.86
210-220 K	**3.9 10^4** 1.1/1.1/1.1	**7.6 10^3** 0.98/0.96/0.95	**5.1 10^3** 0.99/0.97/0.97	/	/
200-210 K	**1.7 10^4** 1.1/1.1/1.1	/	/	/	/

Atmos. Meas. Tech. Discuss., doi:10.5194/amt-2016-345, 2016
Manuscript under review for journal Atmos. Meas. Tech.
Published: 14 November 2016

Atmospheric Measurement Techniques Discussions

Table 6: IIR-MODIS brightness temperature differences in Kelvin at the beginning of the CALIPSO mission and associated uncertainty at the warmest temperature range in each latitude band.

Latitudes Temperatures	IIR1- MODIS29	IIR2- MODIS31	IIR3- MODIS32
30°S-30°N 290-300 K	+0.336 ± 0.001	0.511 ± 0.002	-0.736 ± 0.001
60°S-30°S 280-290 K	0.176 ± 0.001	0.228 ± 0.001	-0.469 ± 0.001
30°N-60°N 280-290 K	0.170 ± 0.002	0.304 ± 0.003	-0.445 ± 0.003
82°S-60°S 270-280 K	0.121 ± 0.002	0.255 ± 0.002	-0.113 ± 0.002
60°N-82°N 270-280 K	0.159 ± 0.003	0.484 ± 0.004	+0.055 ± 0.003

Atmos. Meas. Tech. Discuss., doi:10.5194/amt-2016-345, 2016
Manuscript under review for journal Atmos. Meas. Tech.
Published: 14 November 2016

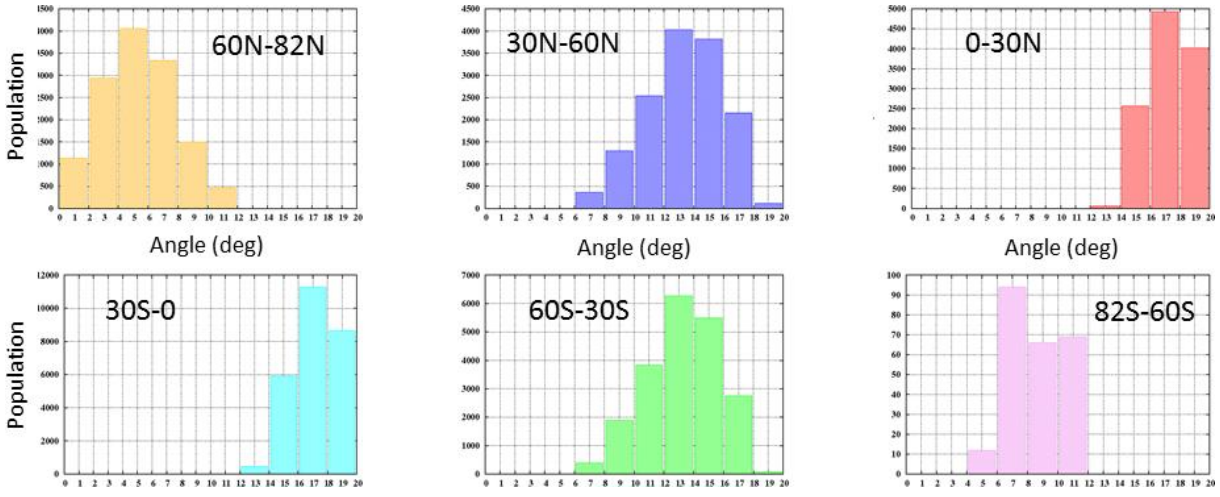

Figure 1: Histograms of MODIS viewing angles for pixels collocated with the IIR swath over ocean in July 2014: Top row from left to right: 60°N-82°N, 30°N-60°N, 0°-30°N; bottom row from left to right: 30°S-0, 60°S-30°S, and 82°S-60°S.

Atmos. Meas. Tech. Discuss., doi:10.5194/amt-2016-345, 2016
Manuscript under review for journal Atmos. Meas. Tech.
Published: 14 November 2016

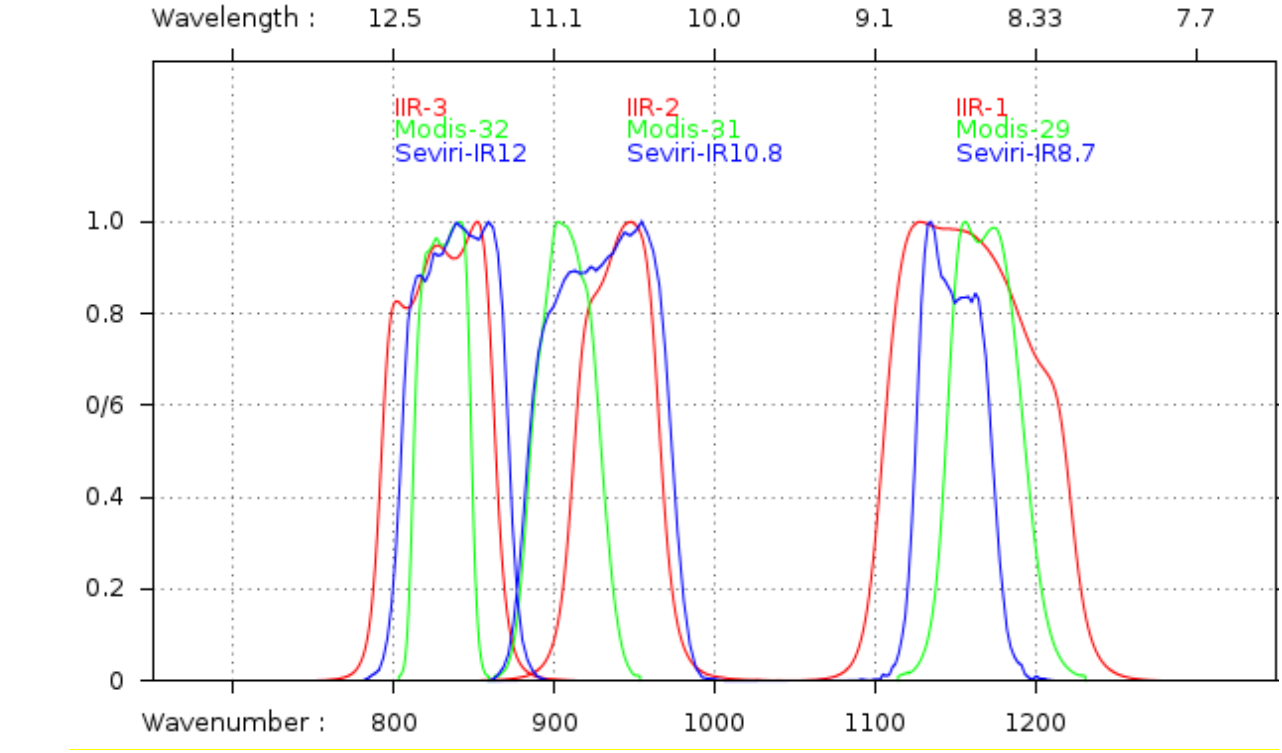

Figure 2: IIR (red), MODIS/Aqua (green) and SEVIRI/Meteosat 8 (blue) Instrument Spectral Response Functions against wavelength in microns (top X-axis) and wavenumber in cm^{-1} (bottom X-axis).

Atmos. Meas. Tech. Discuss., doi:10.5194/amt-2016-345, 2016
Manuscript under review for journal Atmos. Meas. Tech.
Published: 14 November 2016

Atmospheric Measurement Techniques Discussions

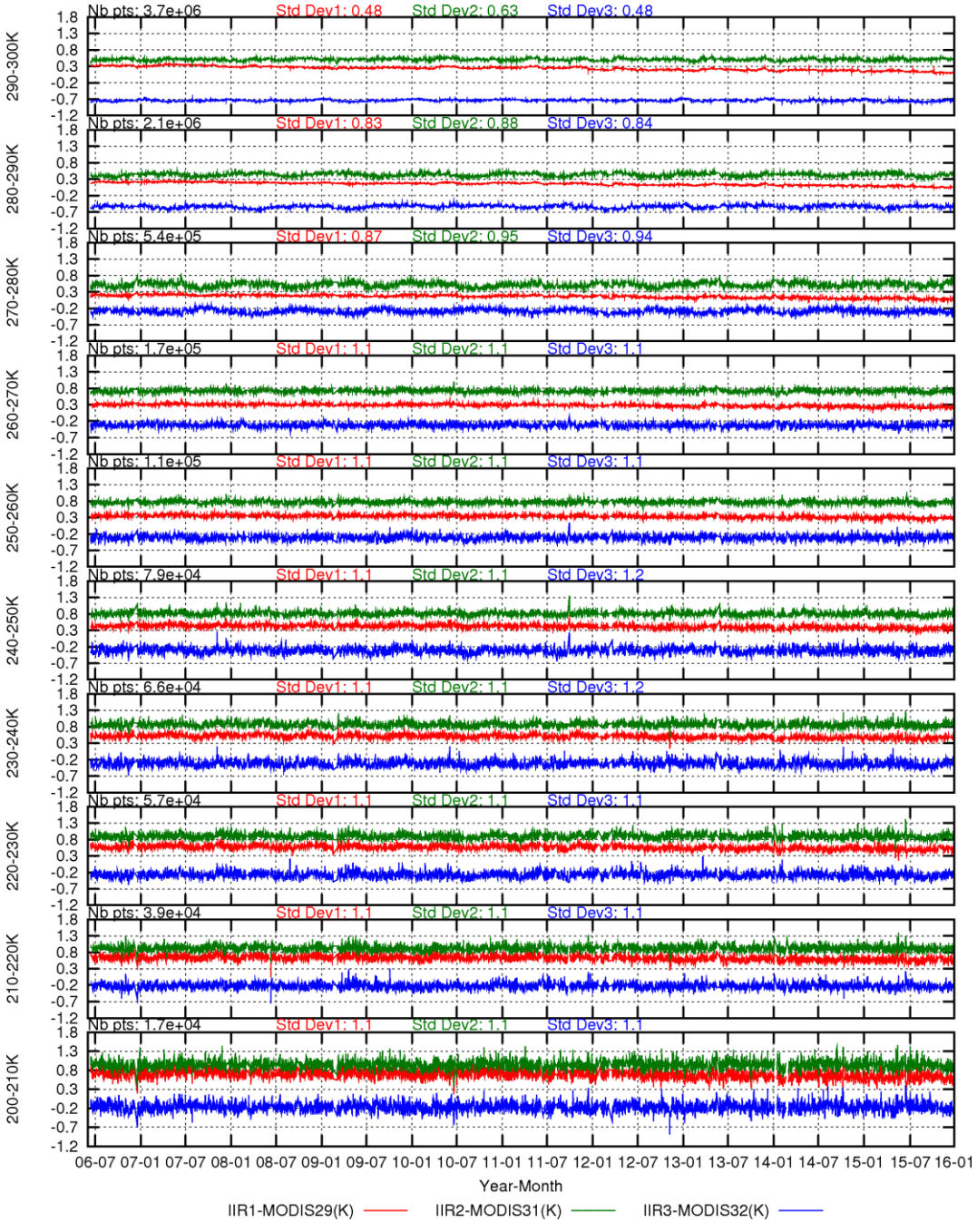

Figure 3: Time series (X-axis: year-month) of IIR-MODIS brightness temperature differences (Y-axis units: Kelvin) for the 3 pairs of companion channels (red: IIR1-MODIS29, green: IIR2-MODIS31, blue: IIR3-MODIS32) over ocean in the tropics at 30°S-30°N. Each panel is for a given range in brightness temperature from 290-300 K (top) down to 200-210 K (bottom). Added at the top of each panel are the mean number of points per day and the mean standard deviation per day for each of the three pairs (see Table 5).

Atmos. Meas. Tech. Discuss., doi:10.5194/amt-2016-345, 2016
Manuscript under review for journal Atmos. Meas. Tech.
Published: 14 November 2016

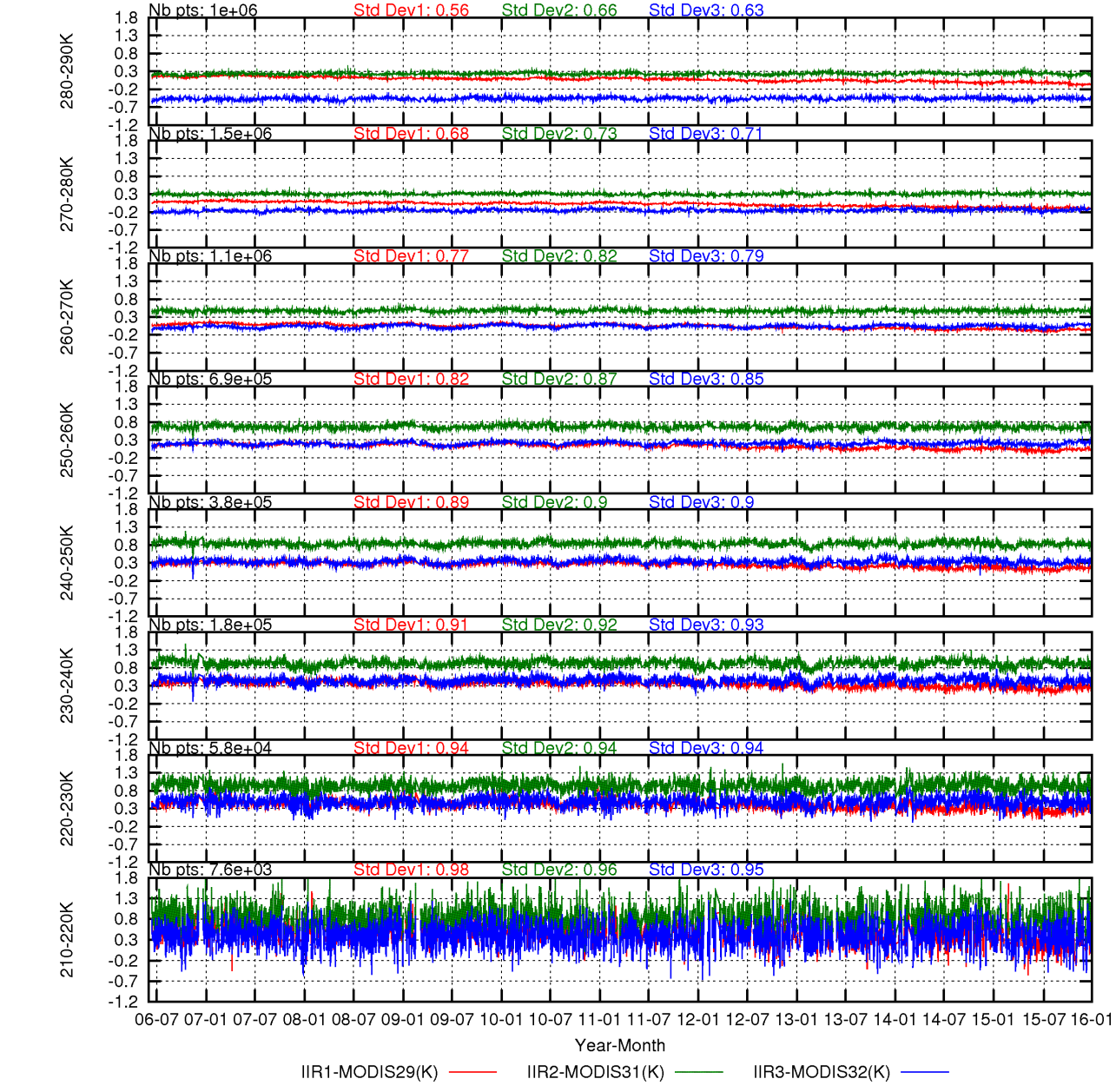

Figure 4: Same as Fig. 3 but at 60°S-30°S. Each panel is for a given range in brightness temperature from 280-290 K (top) down to 210-220 K (bottom).

Atmos. Meas. Tech. Discuss., doi:10.5194/amt-2016-345, 2016
Manuscript under review for journal Atmos. Meas. Tech.
Published: 14 November 2016

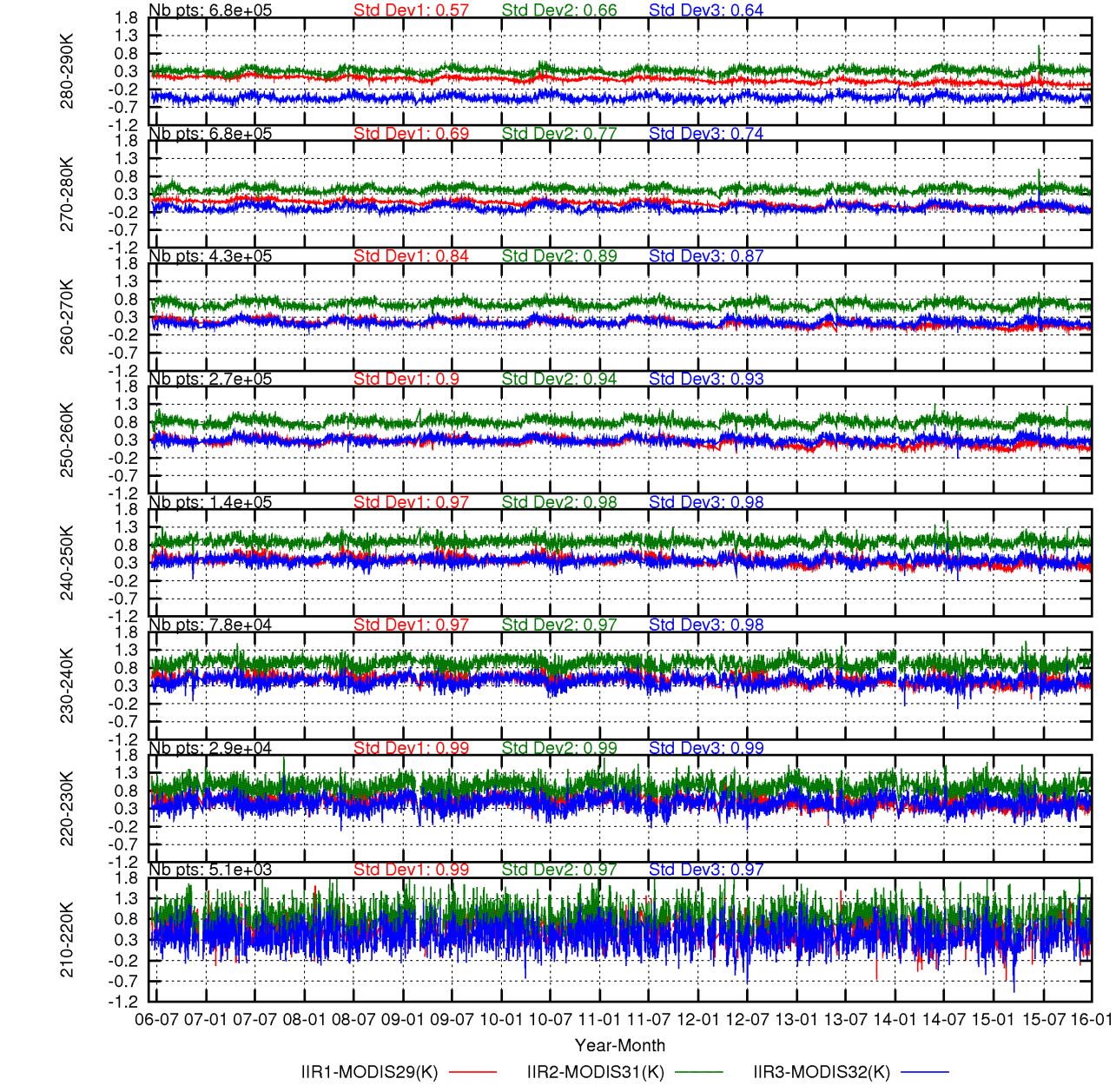

Figure 5: Same as Fig. 4 but at 30°N-60°N.

Atmos. Meas. Tech. Discuss., doi:10.5194/amt-2016-345, 2016
Manuscript under review for journal Atmos. Meas. Tech.
Published: 14 November 2016

Atmospheric Measurement Techniques Discussions

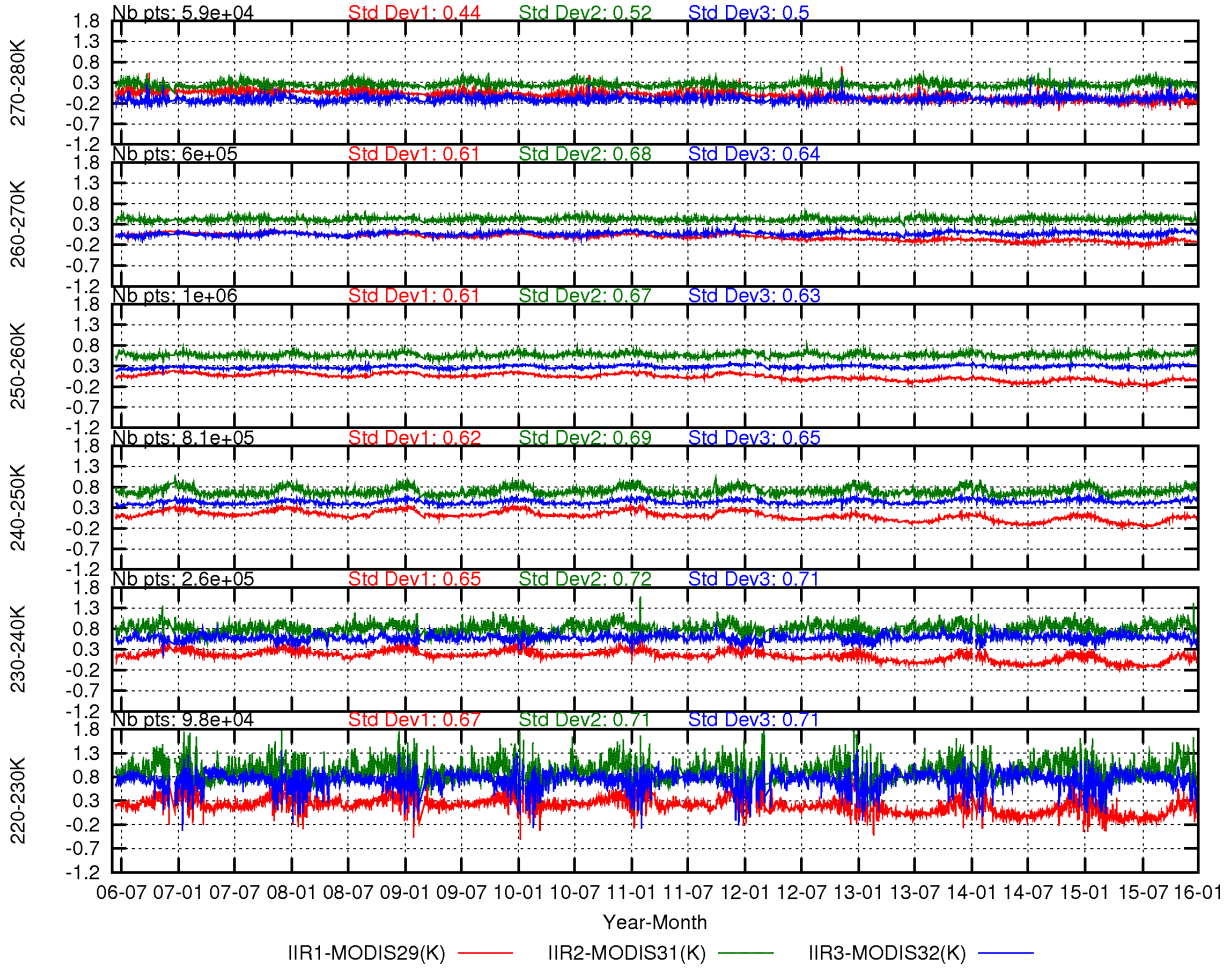

Figure 6: Same as Fig. 3 but at 82°S-60°S. Each panel is for a given range in brightness temperature from 270-280 K (top) down to 220-230 K (bottom).

Atmos. Meas. Tech. Discuss., doi:10.5194/amt-2016-345, 2016
Manuscript under review for journal Atmos. Meas. Tech.
Published: 14 November 2016

Atmospheric Measurement Techniques Discussions

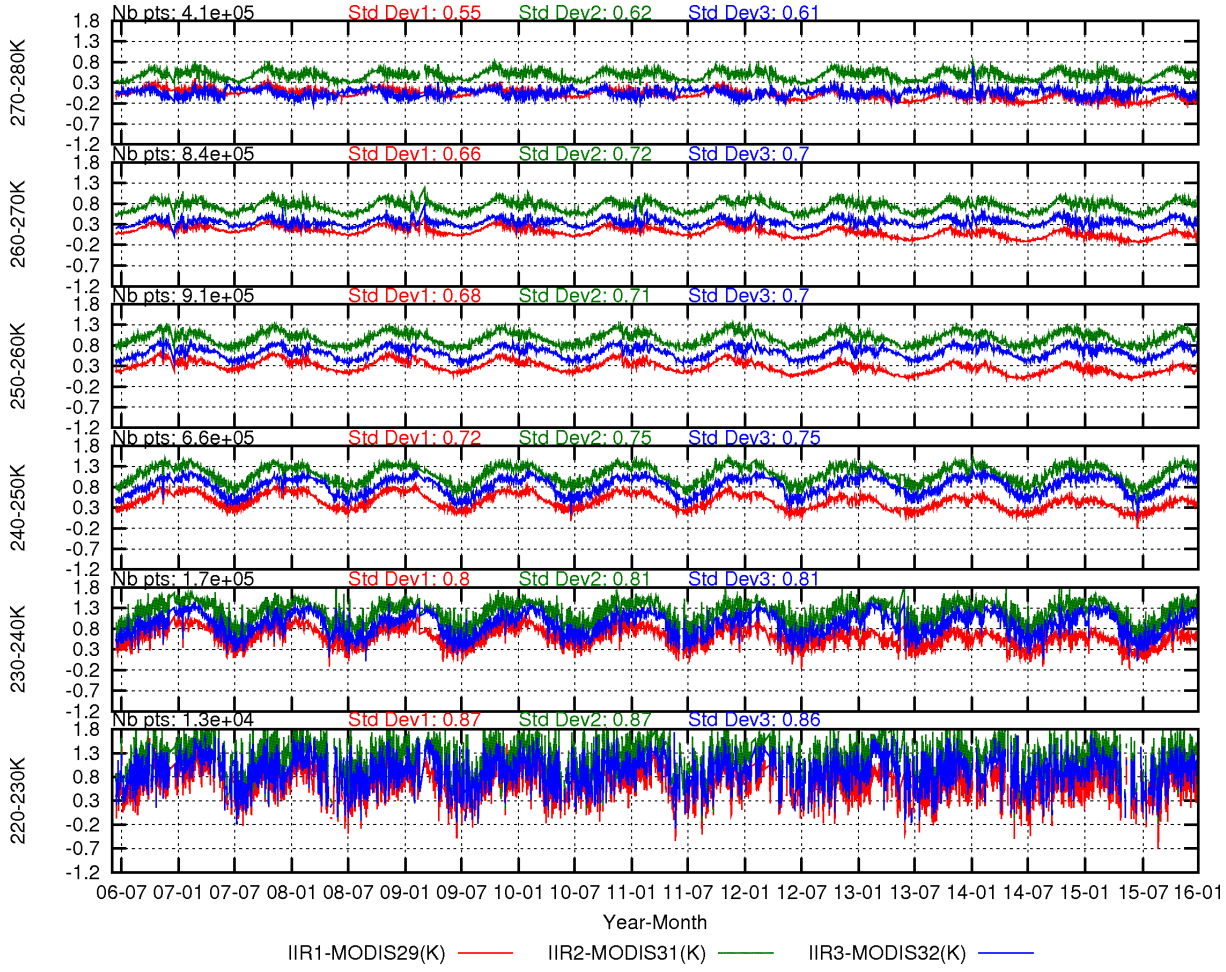

Figure 7: Same as Fig. 6 but at 60°N-82°N.

Atmos. Meas. Tech. Discuss., doi:10.5194/amt-2016-345, 2016
Manuscript under review for journal Atmos. Meas. Tech.
Published: 14 November 2016

Atmospheric Measurement Techniques Discussions

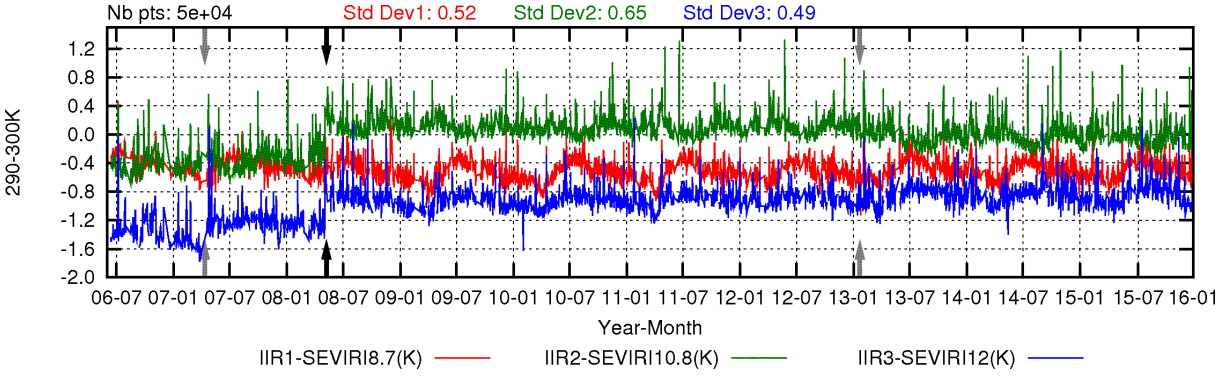

Figure 8: Time series (X-axis: year-month) of IIR-SEVIRI brightness temperature differences (Y-axis units: Kelvin) for the 3 pairs of companion channels (red: IIR1-SEVIRI8.7, green: IIR2-SEVIRI10.8, blue: IIR3-SEVIRI12) over ocean at 290-300 K for SEVIRI viewing angles smaller than 10°. Added at the top of each panel are the mean number of points per day, and the mean standard deviation per day for each of the three pairs. The black arrows indicate the change in the definition of the SEVIRI product in May 2008. The grey arrows indicate the switch from Meteosat 8 to 9 in April 2007 and from Meteosat 9 to 10 in January 2013.

Atmos. Meas. Tech. Discuss., doi:10.5194/amt-2016-345, 2016
Manuscript under review for journal Atmos. Meas. Tech.
Published: 14 November 2016

Atmospheric Measurement Techniques Discussions

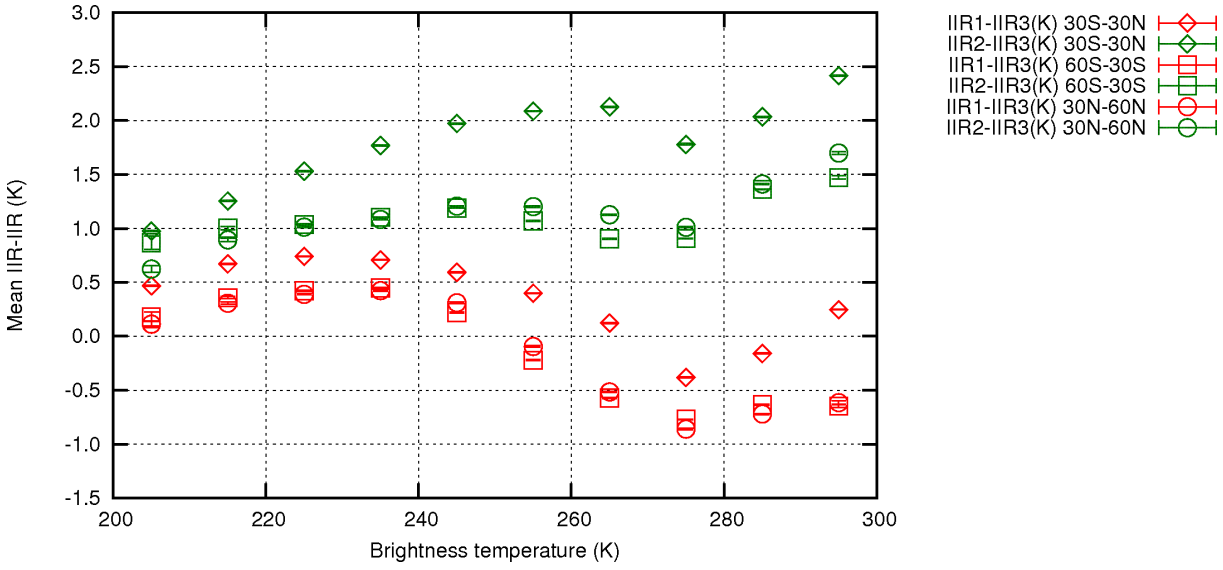

Figure 9: Mean IIR1-IIR3 (red) and IIR2-IIR3 (green) brightness temperature differences and associated uncertainties against temperature. Latitude bands: diamond: 30°S-30°N, square: 60°S-30°S, circle: 30°N-60°N.

Atmos. Meas. Tech. Discuss., doi:10.5194/amt-2016-345, 2016
Manuscript under review for journal Atmos. Meas. Tech.
Published: 14 November 2016

Atmospheric Measurement Techniques Discussions

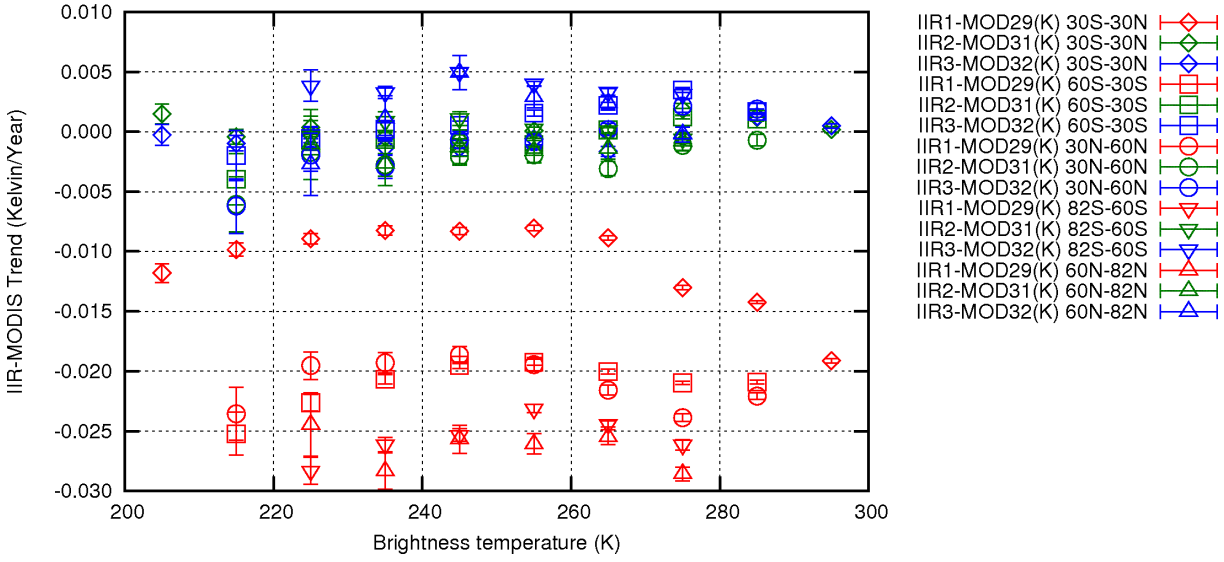

Figure 10: Trends of IIR-MODIS brightness temperature differences and associated uncertainties against temperature for the 3 pairs of companion channels (red: IIR1-MODIS29, green: IIR2-MODIS31, blue: IIR3-MODIS32) as derived from Figs. 3 to 7. Latitude bands: diamond: 30°S-30°N, square: 60°S-30°S, circle: 30°N-60°N, inverse triangle: 82°S-60°S, triangle: 60°N-82°N.

Atmos. Meas. Tech. Discuss., doi:10.5194/amt-2016-345, 2016
Manuscript under review for journal Atmos. Meas. Tech.
Published: 14 November 2016

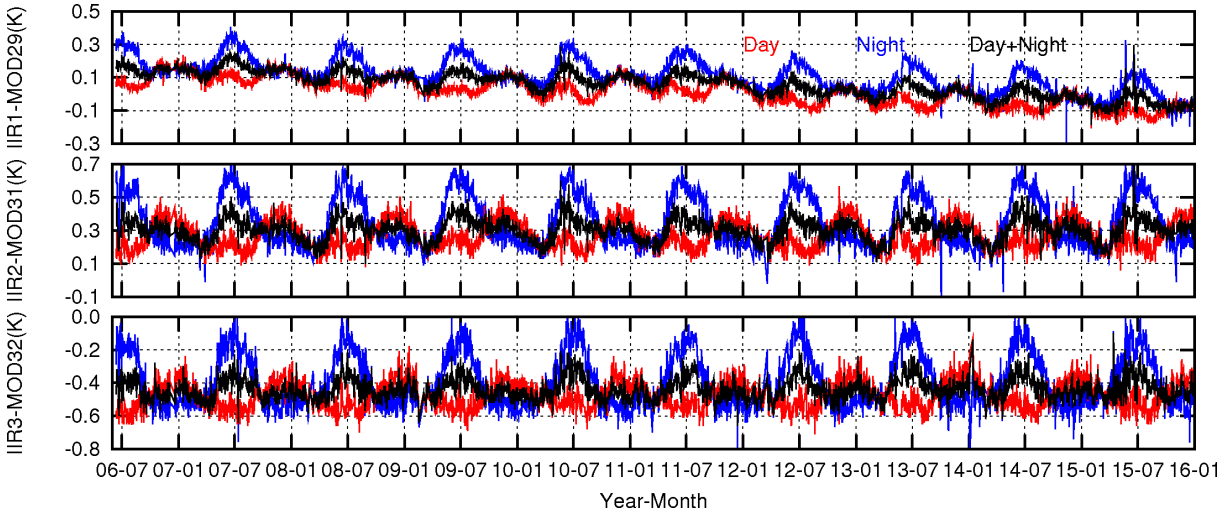

Figure 11: Time series (X-axis: year-month) of IIR-MODIS brightness temperature differences (Y-axis units: Kelvin) for the 3 pairs of companion channels (top: IIR1-MODIS29, middle: IIR2-MODIS31, bottom: IIR3-MODIS32) over ocean at 30°N-60°N and 280-290 K. Red: day only; blue: night only; black: day+night

Atmos. Meas. Tech. Discuss., doi:10.5194/amt-2016-345, 2016
Manuscript under review for journal Atmos. Meas. Tech.
Published: 14 November 2016

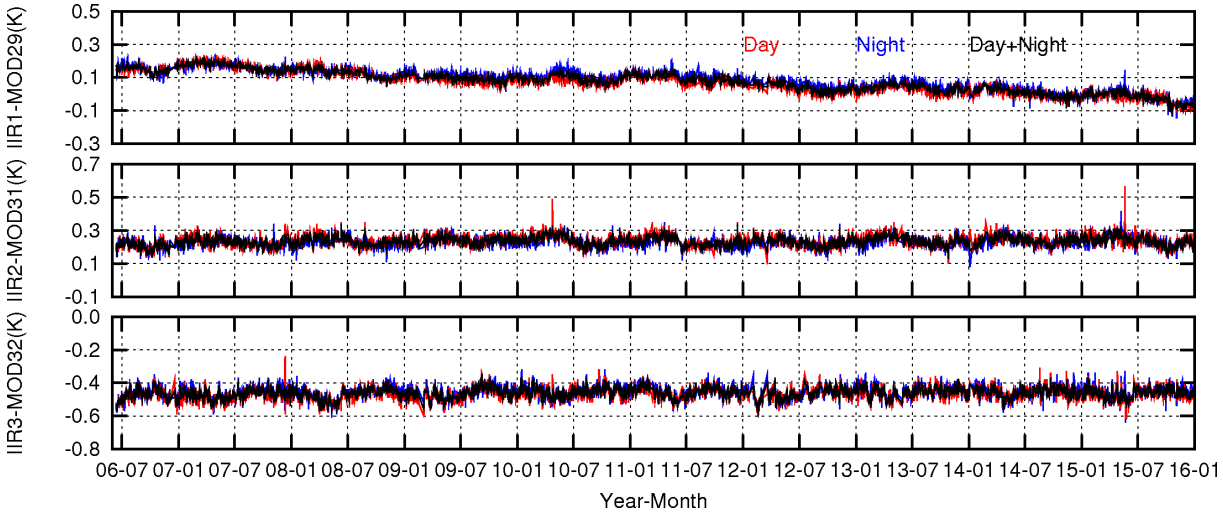

Figure 12: Same as Fig. 11, but at 60°S-30°S.

Atmos. Meas. Tech. Discuss., doi:10.5194/amt-2016-345, 2016
Manuscript under review for journal Atmos. Meas. Tech.
Published: 14 November 2016

Atmospheric Measurement Techniques Discussions

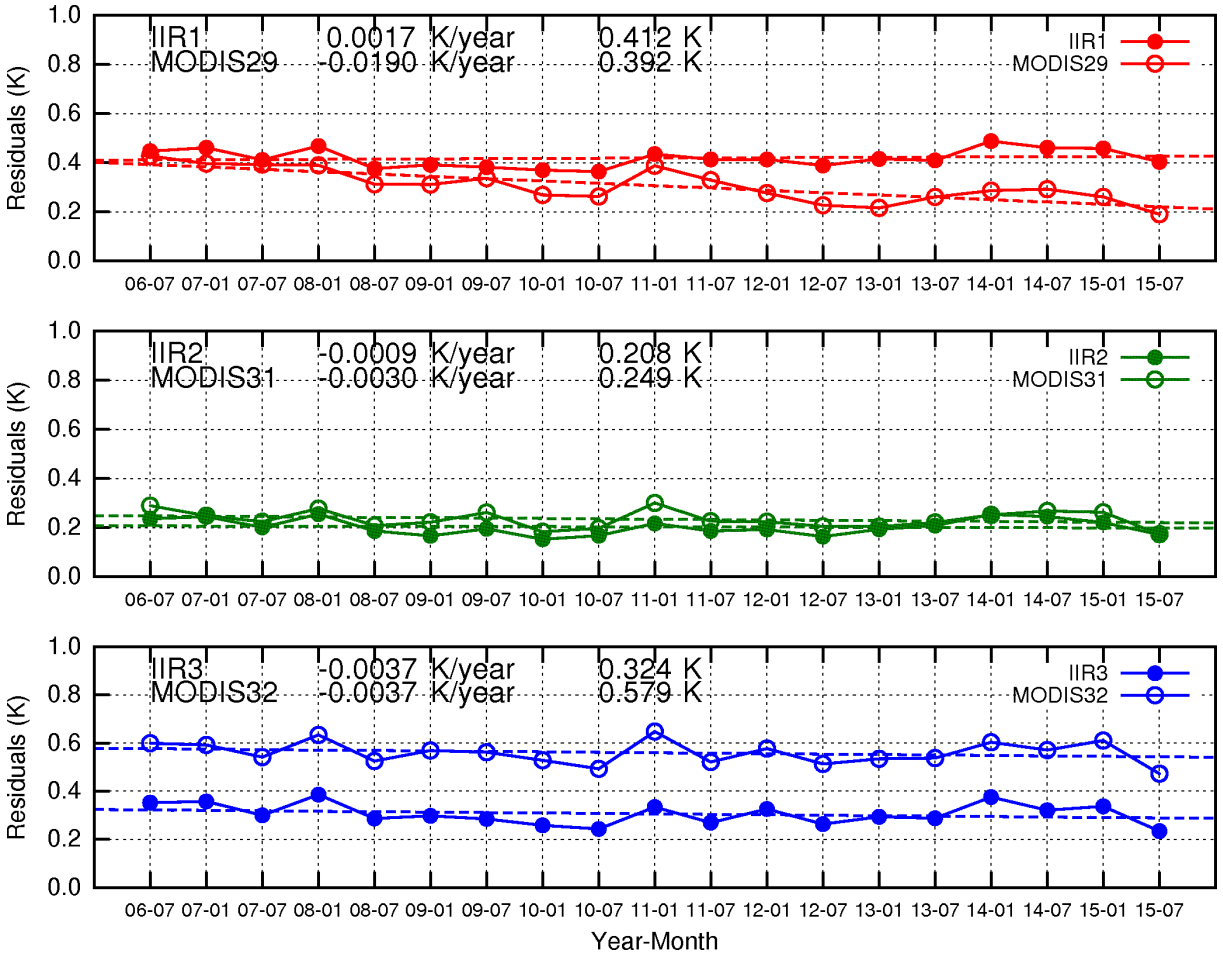

Figure 13: Time series (X-axis: year-month) of residuals (Y-axis units: Kelvin) for the 3 pairs of IIR and MODIS channels (top: IIR1 and MODIS29 in red, middle: IIR2 and MODIS31 in green, bottom: IIR3 and MODIS32 in blue, IIR: full circles, MODIS: open circles) over ocean in the tropics at 30°S-30°N, day and night. Superimposed are linear regressions lines with temporal origin at the beginning of the mission. Slopes (in Kelvin/year) and intercepts (in Kelvin) are given on each panel.

Atmos. Meas. Tech. Discuss., doi:10.5194/amt-2016-345, 2016
Manuscript under review for journal Atmos. Meas. Tech.
Published: 14 November 2016

Atmospheric Measurement Techniques Discussions

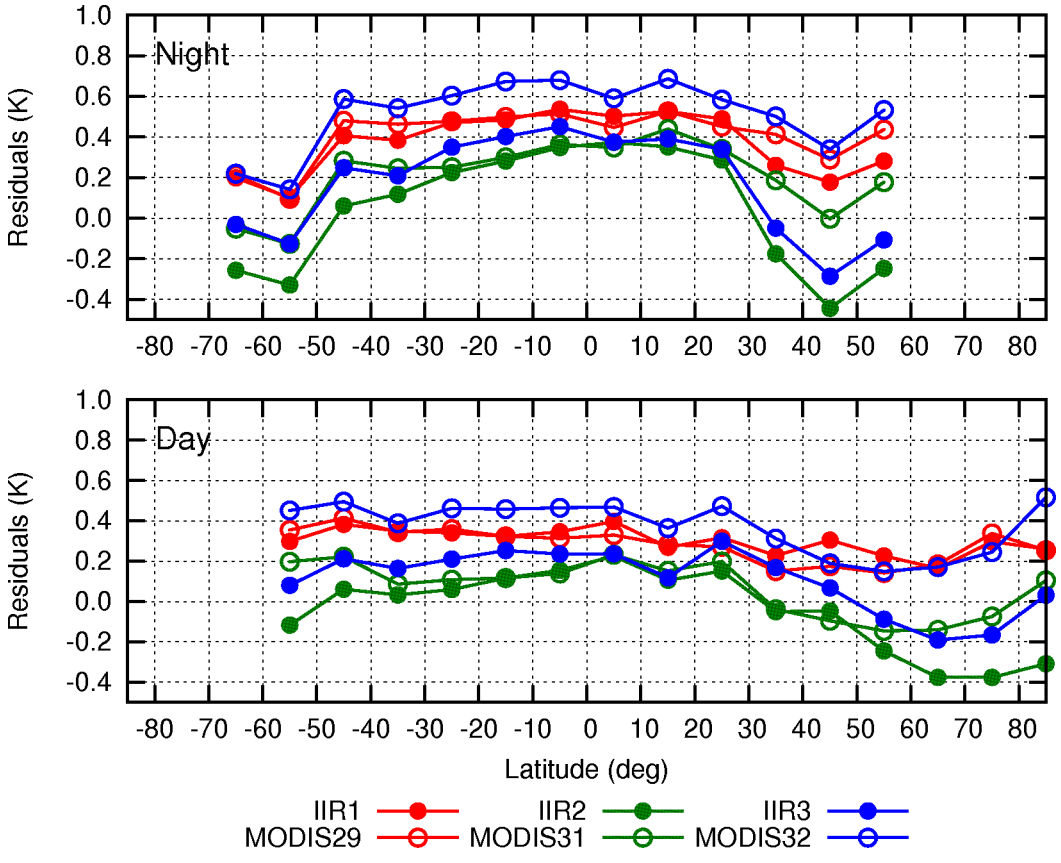

Figure 14: Residuals against latitude in July 2007 for the 3 pairs of IIR and MODIS channels (IIR1 and MODIS29: red; IIR2 and MODIS31: green; IIR3 and MODIS32: blue; IIR: full circles; MODIS: open circles). Top: night; bottom: day.